

Response to the review by Eleni Marinou

Firstly, we want to thank you for your time and effort put into the review of our manuscript. Your careful reading and expert comments are highly appreciated and definitely improve the manuscript.

The main changes in the manuscript are the following:

- The new Fig. 2 presents a sketch to map the MSI grid to JSG and another one which illustrates the search across track by AM-CTH.
- Improved flow charts (Fig. 3 and 4)
- A new subsection describing the AM-ACD validation with *Hawaii* scene. The scene is more complex compared to the rather simple *Halifax aerosol* scene.
- The definition of the quality status of the AM-ACD product was revised.

The answers to your comments are given in bold. In the attached revised version of the manuscript our changes (except some minor grammatical changes) are marked in bold to make it easier for you to spot the new text. For the official revised version, we refer to the manuscript which was separately uploaded to AMT.

The paper presents the AM-COL processor and AM-CTH and AM-ACD products of EarthCARE mission and evaluates their performance using simulated scenes. The paper is of high importance for the exploitation of the EarthCARE mission and falls within the scope of the AMT and the “EarthCARE Level 2 algorithms and data products” special issue. The manuscript is well structured and well written to the majority of its extent. I would suggest the publication of this work after the consideration from the authors to revise the manuscript based on the following comments/suggestions, targeted to improve the clarity of the discussions and results.

General comment:

Along AM-CTH and AM-ACD products, the paper presents the AM-COL processor. It would make sense to include AM-COL in the title as well.

There is the general agreement throughout the EarthCARE special issue to include the product names rather than the processor names in the title. The processors are important for the processing chain and the algorithm developers. However, the main audience of the paper is expected to work with the products and seeks information about how the product was calculated.

EarthCARE Aerosol types: (a) Why in EarthCARE ice is included in the Aerosol types and not in the cloud types? (b) Why do marine and dusty mix have in their name additionally the “aerosol” wording, while not all the other aerosol types? CALIPSO has “marine” and dust mixtures types also, without the “aerosol” addition specifically for this type. Can this be harmonized for EarthCARE aerosol types also? Eg “dust, marine, continental pollution, smoke, dusty smoke, dusty mixtures”?

(a) The aerosol type definition (including ice) is described in Section 2.3.3 and 2.3.4 of the AC-TC paper (Irbah et al., 2023). The ice is considered to indicate the presence of optically thin ice-containing layers (e.g., diamond dust, subvisible cirrus) that have not been identified as clouds and thus occur in the aerosol products (statement from the A-LAY paper, Wandinger et al., 2023b). Following your question which might be the case for many readers, we add a better description:

Lines 249-257: Six aerosol types (dust, marine aerosol, continental pollution, smoke, dusty smoke, dusty aerosol mix) and ice are distinguished in the A-TC product (Irbah et al., 2023). The ice is considered to indicate the presence of optically thin ice-containing layers (e.g., diamond dust, subvisible cirrus) that have not been identified as clouds and thus occur in the aerosol products (Irbah et al., 2023; Wandinger et al., 2023b). If the aerosol type ice amounts to a significant contribution ($> 20\%$ in terms of AOT, configurable) of the column integrated aerosol classification, a cirrus cloud is included in the profile which was not detected by the A-CTH algorithm. The profile is therefore not cloud free and a warning is raised (see quality status in Appendix A2). In the following, only the six aerosol types (excluding the ice) are considered for comparison between ATLID and MSI aerosol classifications

(b) Yes, it is a known issue. The same issue occurred already in the HETEAC paper (Wandinger et al., 2023a), where the aerosol types from the A-PRO processor are discussed as well. We cannot change them in the current paper as it is just using the A-PRO types. By the way, regarding the types, we just use the correct grammatical description. Each aerosol type should be a noun; otherwise you cannot formulate correct sentences. Dust, smoke, and pollution are nouns. Marine and dusty are adjectives and require a noun behind.

Because they are many processors and products discussed in the paper, it would be helpful for the reader if the abbreviations don't change during the different sections of the paper. A confusing example is the AM-CTH product which is presented in Section 3.1 and Figure 2 with this name, while later on in Section 4.1.2 it is discussed both as AM-CTH and "CTH detected by AM-COL", with its legend in the plots in fig 7 (and 8,9,10) to be "CTH AM-COL", and in Section 4.1.3 is discussed as "AM-COL CTH" or "CHT AM-COL". It is advised to describe at first from which processor each product is derived and then continue in the presentation of the flowcharts, plots, and discussions mentioning the product name (eg. AM-CTH for this case). Another case is the M-CLD or MIS CTHs in the text (eg. page 17 line 316 and 374) which in the plots is CTH M-CLD and again it would be nice to be homogenized throughout the manuscript.

You are right. It is confusing to have the processor and product names mixed throughout the paper. Generally, it is better to use the products and not the processors (see answer to your general comment 1). Therefore, I've changed the figures and the text to state, e.g., CTH AM-CTH and CTH M-COP or AOT at 355 nm (AM-ACD). The CTH is the main product of AM-CTH but for consistency I will state CTH AM-CTH.

Specific comments

Page 1, line 20: "Two definitions of the CTH from the model-truth cloud extinction fields are compared": if there is a take-home message from this comparison, it would be interesting to be included in the abstract.

Thank you. We've added the following statement:

Line 22: The geometric CTH is always higher or equal to the radiative CTH.

Page 3, line 71: "The dominant aerosol type can be compared to the aerosol mixing ratios applied in M-AOT." This is confusing, as is not clear what is done. Can this be revised to be more clear? Or else add a note for the reader that this will be presented/discussed in section 3.2.1.

You are right, the statement is confusing for the reader. We improved the whole paragraph to be more precise.

Lines 70-73: The M-AOT algorithm provides aerosol mixing ratios retrieved from MSI observations. The most robust way to compare the ATLID and MSI retrieved aerosol mixing ratios is the comparison of the dominant aerosol type, which is done in the ATLID–MSI Aerosol Column Descriptor (AM-ACD) algorithm.

Page 3, line 71: “The combination of ATLID observations at 355 nm with MSI retrievals for wavelengths ≥ 670 nm (Docker et al., 2023) further supports the aerosol typing.” Is not very clear what/how this is used. Can you elaborate a little? Even if this will be mentioned in any of the 2 papers referred earlier, 1-2 sentence can be useful to the reader. 2

We agree that more details are needed at this point. We were mainly referring to the Ångström exponent. We changed the sentences to the following:

Lines 73-75: The Ångström exponent calculated from the ATLID observations at 355 nm and the MSI retrievals at wavelengths ≥ 670 nm (Docker et al., 2023) further constraints the aerosol typing because the spectral behavior contains information about the particle size.

Page 4, lines 94+: Could you include the Sentinel 5P CTH retrievals in the 2.1 overview? This would be relevant to the reader who may need to use simultaneously EarthCARE and Sentinel 5P/5 for applications (e.g. for data assimilation).

We added a reference to TROPOMI on board the Sentinel-5P and to the future PACE mission (lines 97-99 and 110).

Loyola, D. G., Gimeno García, S., Lutz, R., Argyrouli, A., Romahn, F., Spurr, R. J. D., Pedergrana, M., Doicu, A., Molina García, V., and Schüssler, O.: The operational cloud retrieval algorithms from TROPOMI on board Sentinel-5 Precursor, *Atmospheric Measurement Techniques*, 11, 409–427, <https://doi.org/10.5194/amt-11-409-2018>, 2018.

Compernelle, S., Argyrouli, A., Lutz, R., Sneep, M., Lambert, J.-C., Fjæraa, A. M., Hubert, D., Keppens, A., Loyola, D., O'Connor, E., Romahn, F., Stammes, P., Verhoelst, T., and Wang, P.: Validation of the Sentinel-5 Precursor TROPOMI cloud data with Cloudnet, Aura OMI O2–O2, MODIS, and Suomi-NPP VIIRS, *Atmospheric Measurement Techniques*, 14, 2451–2476, <https://doi.org/10.5194/amt-14-580-2021>, 2021.

Sayer, A. M., Lelli, L., Cairns, B., van Diedenhoven, B., Ibrahim, A., Knobelspiesse, K. D., Korkin, S., and Werdell, P. J.: The CHROMA cloud-top pressure retrieval algorithm for the Plankton, Aerosol, Cloud, ocean Ecosystem (PACE) satellite mission, *Atmospheric Measurement Techniques*, 16, 969–996, <https://doi.org/10.5194/amt-16-969-2023>, 2023.

Page 5, line 142: “wind lidar mission Aeolus”: It would be nice if you could add a reference here for Aeolus mission or Aladin lidar.

We added the following reference (line 146):

Stoffelen, A., Pailleux, J., Källén, E., Vaughan, J. M., Isaksen, I., Flamant, P., Wergen, W., Andersson, E., Schyberg, H., Culoma, A., Meynart, R., Endemann, M., and Ingmann, P.: The Atmospheric Dynamics Mission for Global Wind Field Measurement, *Bulletin of the American Meteorological Society*, 86, 73 – 88, <https://doi.org/10.1175/BAMS-86-1-73>, 2005.

Page 7, lines 162-164: “The A-LAY products ... are already provided on JSG with this resolution (approximately 1 km) along track ... The MSI products ... are provided on the finer resolution of the MSI grid (500 m)... The surrounding nine MSI pixels correspond to one JSG

pixel”: With 1 center pixel and 8 surrounding pixels (9 in total) of 500 m JSG would have 1.5 km resolution. How can 9 surrounding pixels of 500 m correspond to 1 km JSG along track? Maybe an explanatory diagram would clarify this question.

A good idea. We’ve added a new figure (Fig. 2a) to illustrate how the MSI grid is mapped to JSG.

Figure 2: *It would be very helpful to the reader if the flowchart is more detailed, including not only the steps followed but also the decisions in each step. So one can get from the flowchart all the information for which pixels AM-CTH data are provided and how.*

We agree. Figure 2 (now Fig. 3) was improved to clearly show which decisions are made by the algorithm. Overlapping lines are eliminated.

Page 10, line 227: *“(default 75 pixels in each direction along track)”. Can you include here the distance in km this refers to? In MSI grid, this would mean 37.5 km along the track, in JSG grid of 1 km, this would mean 75 km.*

We clarified the statement:

Lines 231-232: (default 75 JSG pixels (approximately 75 km) in each direction along track)

Additionally, we added Fig. 2b to illustrate the process.

Page 10, lines 225-229: *The search for agreement starts at the closest along-track pixel. It continues by searching one pixel before ...and one pixel after ... from the closest pixel along track ... This alternating search is continued until an agreement is found or the configurable maximum search distance ... is reached. If a measurement at swath fits to an along-track measurement for all criteria, then the observed CTH difference from the track is assigned to the swath pixel”. When reading this part is a little confusing. Only for this one swath pixel the CTH difference is assigned? And then the search for agreement stops for a more far-away grid? Please revise if it is not the case and all pixels are searched until a disagreement is found (which would be the expected case).*

The search is done for every across-track pixel individually. If an agreement was found, the next across-track pixel is taken, and so on. If no agreement was found, no CTH difference is assigned to the pixel. Neighboring pixel are not considered. In the revised version, Fig. 2b and the decision tree in Fig. 3 are added to make clear how the search is done. In the caption of Fig. 2b it is written:

“The sketch illustrates the transfer of the CTH difference from the track to the swath. For an across-track pixel, first the nearest along-track is compared (5 or 3 criteria, see Fig. 3). If no agreement was found, the search continues alternating North (n-1) and South (n+1) of the closest along-track pixel until agreement is found or a configurable maximum search distance is reached. Then, the process is repeated for the next across-track pixel.”

Figure 3: *Same suggestion as for figure 2.*

Figure 3 (now Fig. 4) was redesigned to better show the steps which are made by the AM-ACD algorithm.

Page 11, line 243: “Seven aerosol types (dust, marine aerosol, continental pollution, smoke, dusty smoke, dusty aerosol mix, ice)...” This is very confusing. Why ice is in aerosol types and not in cloud types? Is this the case for the EarthCARE Aerosol type product? Why it couldn't be included in the cloud types, as is the case of CALIPSO?

At this point, we refer to our answer to your general comment 2. Here a quote from Irbah et al., 2023 (AC-TC paper) is provided:

Ice crystals are also treated as an aerosol type, since they span part of the δ -S parameter space not occupied by aerosols (see Fig. 3). This is used to further refine the separation between thin ice clouds from aerosol fields. This is required, since the backscatter-threshold-based cloud aerosol separation step applied earlier tends to produce halos of aerosol around upper-level ice clouds. (Irbah et al., 2023)

Page 11, line 243: “Seven aerosol types (dust, marine aerosol, continental pollution, smoke, dusty smoke, dusty aerosol mix, ice)...” Why marine and dusty mix have in their name additionally the “aerosol” wording, while not all the other aerosol types? CALIPSO has “marine” and dust mixtures types also, without the “aerosol” addition specifically for this type. Can this be harmonized for EarthCARE aerosol types also? Eg “dust, marine, continental pollution, smoke, dusty smoke, dusty mixtures”?

Please see our answer above to your general comment 2.

Page 11, line 243: “Seven aerosol types (...) are distinguished”. Here it would be useful to mention from which processor and in which product the aerosol types are provided.

Thank you. We added an improved description (see next comment).

Page 11, line 244: “If the aerosol type ice dominates the column integrated aerosol classification, a cirrus cloud is included in the profile which was not detected by the A-CTH algorithm”. (a) This is very confusing. If there is an ice cloud, it should be included in the A-CTH product and not be treated from the AM-CTH. And not in the Aerosol types. Why this is not the case? (b) You state that “If the aerosol type ice dominates...”. If ice is present but doesn't dominated, is the pixel again excluded? I believe it should be.

You're right. If the ice contribution is larger than a configurable threshold (default 20% in terms of AOT), a warning is raised. Ice must not be dominating but having a significant contribution is enough to exclude it from the AM-ACD algorithm. However, it is not put into the AM-CTH algorithm because this algorithm runs before AM-ACD. The manuscript was improved to address this and the previous comment:

Lines 249-257: Six aerosol types (dust, marine aerosol, continental pollution, smoke, dusty smoke, dusty aerosol mix) and ice are distinguished in the A-TC product (Irbah et al., 2023). The ice is considered to indicate the presence of optically thin ice-containing layers (e.g., diamond dust, subvisible cirrus) that have not been identified as clouds and thus occur in the aerosol products (Irbah et al., 2023; Wandinger et al., 2023b). If the aerosol type ice amounts to a significant contribution (> 20% in terms of AOT, configurable) of the column integrated aerosol classification, a cirrus cloud is included in the profile which was not detected by the A-CTH algorithm. The profile is therefore not cloud free and a warning is raised (see quality status in Appendix A2). In the following, only the six aerosol types (excluding the ice) are considered for comparison between ATLID and MSI aerosol classifications.

Page 12, of section 3.2.1 and Table 3: With the description provided on this page for section 3.2.1, it is not clear how the comparison will reach agreement or not. Can Table 3 be enhanced with the used thresholds of the agreement for each A-TC type? Also, can one column with the M-AOT aerosol classification be included in the Table?

The M-AOT aerosol classification uses the 4 aerosol components of HETEAC. In Docter et al., 2023, a table defines the 25 precalculated mixtures of the 4 HETEAC aerosol components. If one of 4 basic aerosol components dominates the mixture in the M-AOT product and the corresponding A-TC aerosol type dominates the columnar aerosol classification probabilities in the A-ALD product, agreement is reached. Here, no thresholds are necessary. The thresholds get necessary when it comes to the mixed aerosol types in A-TC.

We tried to make it clearer throughout the subsection by pointing to M-AOT. Another column in the table seems not to be necessary, as M-AOT uses exactly the four basic aerosol components defined in HETEAC. The comparison would have been easier, if A-TC would have used the 4 HETEAC aerosol components instead of the 6 aerosol types which are mixtures of the HETEAC aerosol components.

Page 13, line 268: “If the dominant aerosol type agrees (see Sect. 3.2.1)”. It would be helpful in this section to mention how the dominant aerosol type is defined. Eg., the M-AOT HETEAC component with the biggest %?

Thank you for pointing to this issue. We improved the code in the way, that the Ångström exponent is calculated for the 6 (A-TC) aerosol types along track. Across track, the dominant aerosol type is determined from the 4 HETEAC aerosol components according to the description in Sect. 3.2.1 (4 pure types are mapped directly, for the mixtures the thresholds are applied. We added a definition of the dominant aerosol type:

Line 264: The dominant aerosol type is defined by the highest columnar aerosol classification probability (A-ALD product).

Figure 6: How y axis density is calculated? Scaled to the total number of pixels for every case, with 1 as a cumulative sum? Maybe is worth mentioning it. Also, the colorbar in model truth comparison plot (and relevant plots from there on) can use a legend/units (eg. nr pixels).

Thank you for your comment. Indeed, we revised the legend and changed the plotting from density (where it is normalized to sum of all pixel) to number of pixels. Now, it get's clear that AM-CTH provides values for approximately half of the cloudy pixels detected by M-CM. Therefore, the number of counts in brackets was removed. A caption was also given to the color bar in the scatter plots.

Page 17, lines 375-376: “Especially the cirrus clouds between 9 and 13 km height are detected by AM-CTH above a COT of 0.25”. This is confusing. From Figure 6 I would conclude that the cirrus clouds between 9 and 13 km height are detected by AM-CTH below a COT of 0.25. But maybe there is something else you wanted to highlight. Please rephrase to make it clear.

Sorry, thank you for pointing to it. It should be written “below a COT of 0.25”. We changed it.

Page 18, line 378: “The amount of data points within an interval of $\pm i$ m around the 1:1 line (fi in Fig. 7 and 8) shows a similar behavior for AM-COL to extinction-based model truth (40, 63, 83% for 300, 600, 1500 m) and M-CLD to COT-based model truth (31, 53, 77% for 300, 600, 1500 m)”. Earlier in the manuscript (page 17 line 366) was mentioned that “40% are within ± 300 m which was defined in the mission requirements”. Does the statistics on page 18 show

us that only the AM-COL is within the mission requirements, while the M-CLD isn't? Please consider if you would like to highlight it in this part of the paper.

The aim of this statement is to show that AM-CTH provides you the geometric CTH obtained by the extinction threshold and M-COP provides the radiative CTH as obtained by the COT threshold. At this point the mission requirements are not accurately enough as they state just CTH. Nevertheless, I would prefer the geometric definition when talking about CTH. Therefore, AM-CTH better fulfills the mission requirements. However, M-COP is needed to provide information besides the track. Therefore, we do not want to emphasize that just one processor is within the mission requirements. The combination of both instruments brings the best results – along with the synergistic approach of EarthCARE. We have not changed the text at this point.

Page 22, line 418: “Thus, the dominant”. Why thus? Could it be the case that the classifications are not so successful, hence “thus” is not correct? Or there is a connection between the simplicity of the scene and the fact that the classifications are successful? If possible, modify the text to make it clear.

Thank you. We deleted the word “Thus”.

Page 22, lines 420-422: “The ice cloud at 34°N was only partly detected by the MSI cloud mask and thus the AOT of the ice crystals is included in the M-AOT product”. One wouldn't expect to find ice OD in AOT products. Why this is not the case for EarthCARE products?

The reason is simply that the pixels were marked as cloud-free by M-CM and therefore the aerosol processor M-AOT was applied to them. The ice crystals contribute to the optical depth and M-AOT retrieves the optical depth for the pixels which were classified as cloud-free. But you're right the word AOT is not correct in this sentence. We've changed it to:

Lines 448-449: The ice cloud at 34°N is only partly detected by the MSI cloud mask and thus the optical thickness of the ice crystals is included in the M-AOT product.

Page 22, line 420-422: “Here, as well the ice crystals are included in the AOT, which differs from the CAMS model truth AOT provided for aerosol only”. Please revise to improve the syntax.

Thank you. We revised the statement:

Lines 450-452: The additional optical thickness of the ice crystals increases the AOT in the A-ALD product and lead to an overestimation compared to the CAMS model truth AOT which is provided for aerosol only.

Figure 12: Can you comment on why some values (with the highest AOT) are flagged out in the 355 nm AOT, although some seem to have quality status = 0?

Thank you for your careful look. Indeed, the quality status was not well defined. We've improved the algorithm and the manuscript. Now, the quality status for AM-ACD is defined as:

QACD = 0: Good data, high quality of M-AOT input.

QACD = 1: Warning: A significant amount of ice (> 20% (configurable) in terms of AOT) was detected by A-TC (provided in A-ALD). This warning is provided along track only, but probably holds for the close swath pixel as well.

QACD = 2: Warning: Dominant aerosol type on swath was not present along the track, AOT at 355 nm could not be calculated.

QACD = 3: Warning: The homogeneity criteria of M-AOT are not fulfilled.

QACD = 4: Bad data. Observations on MSI grid are not consistent on JSG.

QACD = -1: Not surely cloud free according to M-CM.

And Fig. 12 (now Fig. 14) was updated accordingly.

Page 22-23, lines 434-439: “The derived ...at 607 nm”. Is there an error estimation for this new product (AM-ACD AOT 355)? If yes, does it consider/include the uncertainty due to the Ångström exponent bias mentioned?

Yes, there is an error estimation of the AM-ACD AOT at 355 nm. The uncertainty of the Ångström exponent was included as an additional source of uncertainty for the product. However, the bias of the Ångström exponent is only known for the simulated test scenes. It won't be the case for real world data.

Page 35, lines 469-470: “However, the brightness temperature difference between 10.8 and 12.0 μm was not sensitively enough simulated to clearly detect multi-layer cloud scenarios by MSI.” I believe that the brightness temperature sensitivity is not discussed earlier when the results from the multi-layer cloud scenarios are presented. It would be interesting to include a comment on this in the earlier session also.

A further sentence was added in the subsection 4.1.3 (AM-CTH algorithm performance for different cloud classes) when the multilayer cloud detection was described.

Lines 408-410: However, the brightness temperature difference between 10.8 and 12.0 μm was not sensitively enough simulated in the EarthCARE test scenes to clearly detect multi-layer clouds with MSI.

Page 27: “QCTH = 4: Bad data. Observations on MSI grid are not consistent on (coarser) JSG”. Coarser JSG is not defined in the text. Can you define it here?

The resolution of the Joint Standard Grid (JSG) is coarser than the one of the MSI grid. However, there is only one JSG and no “coarser JSG”. We deleted the word “coarser”.

Technical corrections/suggestions (bold text & red “,:”):

Your careful reading is highly appreciated. We followed your suggestions in the revised version.

Page 1, line 1: “is a combination of multiple active...”.

Page 1, line 6: “characterize the 3-dimensional scene”, a suggestion to change to “characterize a 3-dimensional scene”, or “characterize the 3-dimensional scenes”.

Page 1, line 7: “(A-LAY), ~~and the~~ MSI L2a data from the MSI Cloud Products processor (M-CLD), ~~and~~ [here we kept the ‘and’] the MSI Aerosol Optical Thickness processor (M-AOT), as well as MSI Level 1c (L1c) data are used as input to produce the synergistic columnar products”.

Page 1, line 14: “CTH detected by ATLID ~~and retrieved/provided~~ MSI is calculated”: retrieved or provided by MSI is a more representative term for this product.

Page 1, line 18: "The quality status depending on day/night conditions or the presence of multiple cloud or aerosol layers is provided with the products". The syntax could be improved.

Page 2, line 34: "~~a~~ three-dimensional (3D) scenes (e.g., Qu et al., 2022a; Mason et al., 2022) to calculate ~~the~~ radiative fluxes which ~~is~~ **are** compared..".

Page 2, line 40: "about the scene ~~apart from~~ **around** the satellite track".

Page 3, line 46-48: "It provides vertical profiles along the satellite track of the particle backscatter and extinction coefficient, the lidar ratio, and the particle linear depolarization ratio which are **provided stored** in the ATLID L2a product A-EBD". Suggestion because they are 2 provided in 1 sentence and is less clear.

Page 3, line 52-53: "(et al., 2022), and to retrieve cloud optical properties such as the cloud optical thickness (COT), CTH and the effective radius of the cloud droplets which ~~is~~ **are** provided in the MSI Cloud Optical and Physical product".

Page 3, line 56: "for ~~the~~ **a** 3D scene". Is it a requirement for this scene presented in the paper, or for overall the scenes? If the 2nd "a" is needed there.

Page 3, line 9:"**a** reasonable estimates".

Page 4, line 84: " using ~~the~~ common test scenes".

Page 4, line 86: "Conclusions"

Page 4, line 96: "with lidars **as for example** from the Cloud-Aerosol Lidar and Infrared Pathfinder Satellite Observations": CALIPSO is not the only lidar that has been used for CTH detection.

Page 4, line 100: "in dependence **on of** the type".

Page 4, line 105: "the CTH ~~for~~ **of** high".

Page 5, line 119: "not from ~~the~~ **a** space lidar".

Table 1: "and the products (~~with references~~) in which they are contained (**bold, with references**)".

Page 7, line 158: "...after the ~~complete~~ ATLID L2a and MSI L2a processing is completed".

Page 8, line 180: " **Then** the scene...".

Page 10, line 234: "over ocean), **and** the respective Ångström exponents, and their uncertainties".

Page 14, lines 299-300: "**And more specifically w**With the EarthCARE End-to-End Simulator specific test scenes **which** were created to test the full chain of EarthCARE processors". Something is missing in this sentence. A possible suggestion.

Page 14, line 327: "There are several reasons:": It would read better if you clarify after this text the reasons. Eg. "reasons of failure" "reasons AM-CTH can't be retrieved".

Page 15, line 340: "The central question is,: how to define the CTH from the true cloud extinction fields?".

Cloud top heights and aerosol columnar properties from combined EarthCARE lidar and imager observations: the AM-CTH and AM-ACD products

Moritz Haarig¹, Anja Hünnerbein¹, Ulla Wandinger¹, Nicole Docter², Sebastian Bley¹, David Donovan³, and Gerd-Jan van Zadelhoff³

¹Leibniz Institute for Tropospheric Research (TROPOS), Leipzig, Germany

²Free University of Berlin (FUB), Institute for Space Science, Berlin, Germany

³Royal Netherlands Meteorological Institute (KNMI), De Bilt, The Netherlands

Correspondence: Moritz Haarig (haarig@tropos.de)

Abstract. The Earth Cloud, Aerosol and Radiation Explorer (EarthCARE) is a combination of multiple active and passive instruments on a single platform. The Atmospheric Lidar (ATLID) provides vertical information of clouds and aerosol particles along the satellite track. In addition, the Multi-Spectral Imager (MSI) collects the multispectral information from the visible till the infrared wavelengths over a swath width of 150 km across the track. The ATLID–MSI Column Products processor (AM-
5 COL) described in this paper combines the high vertical resolution of the lidar along track and the horizontal resolution of the imager across track to better characterize a 3-dimensional scene. ATLID Level 2a (L2a) data from the ATLID Layer Products processor (A-LAY), MSI L2a data from the MSI Cloud Products processor (M-CLD) and the MSI Aerosol Optical Thickness processor (M-AOT), as well as MSI Level 1c (L1c) data are used as input to produce the synergistic columnar products: the ATLID–MSI Cloud Top Height (AM-CTH) and the ATLID–MSI Aerosol Column Descriptor (AM-ACD). The coupling of
10 ATLID (measuring at 355 nm) and MSI (at ≥ 670 nm) provides multispectral observations of the aerosol properties. Especially, the Ångström exponent from the spectral aerosol optical thickness (AOT 355 nm/670 nm) adds valuable information for aerosol typing. The AOT across track, the Ångström exponent and the dominant aerosol type are stored in the AM-ACD product. The accurate detection of the Cloud Top Height (CTH) with lidar is limited to the ATLID track. The difference of the CTH detected by ATLID and **retrieved by** MSI is calculated along track. The similarity of MSI pixels across track with those along track
15 is used to transfer the calculated CTH difference to the entire MSI swath. In this way, the accuracy of the CTH is increased to achieve the EarthCARE mission goal aiming to derive the radiative flux at the top of the atmosphere with an accuracy of 10 W m^{-2} for a 100 km^2 snapshot view of the atmosphere. The synergistic CTH difference is stored in the AM-CTH product. **The quality status is provided with the products. It depends, e.g., on day/night conditions and the presence of multiple cloud layers.** The algorithm was successfully tested using the common EarthCARE test scenes. Two definitions of the CTH
20 from the model-truth cloud extinction fields are compared: An extinction-based threshold of 20 Mm^{-1} provides the geometric CTH and a cloud-optical-thickness threshold of 0.25 describes the radiative CTH. The first one detected with ATLID, the second one with MSI. **The geometric CTH is always higher or equal to the radiative CTH.**

1 Introduction

Clouds and aerosol particles have a major influence on the radiation budget of the Earth as they interact with incoming solar radiation and outgoing terrestrial radiation. However, their global distribution is highly variable in time and space. Additionally, their vertical distribution is essential to accurately calculate their role in the radiation budget. To improve the global observation capabilities and the radiation models, the Earth Cloud, Aerosol and Radiation Explorer (EarthCARE) mission was designed (Illingworth et al., 2015). The European Space Agency (ESA) and the Japan Aerospace Exploration Agency (JAXA) built a satellite with four instruments on one single platform: a Cloud-Profiling Radar (CPR), an Atmospheric Lidar (ATLID), a Multi-Spectral Imager (MSI) and a Broadband Radiometer (BBR) (Illingworth et al., 2015; Wehr et al., 2023). The innovation of having two active (CPR, ATLID) and two passive (MSI, BBR) instruments on a single platform enables a highly synergistic approach in characterizing the state of the atmosphere. It is an unprecedented observational setup which will offer novel opportunities in atmospheric research beyond the initial mission goals. CPR, ATLID and MSI are used to retrieve three-dimensional (3D) scenes (e.g., Qu et al., 2023; Mason et al., 2023b) to calculate radiative fluxes which are compared to the radiometer (BBR) measurements on board (Barker et al., 2023). The European and Canadian EarthCARE processing chain is presented by Eisinger et al. (2023). The need to derive the radiative flux at the top of the atmosphere with an accuracy of 10 Wm^{-2} for a 100 km^2 snapshot view of the atmosphere is the leading idea for the EarthCARE mission requirements (MRD, 2006). The vertical profiles of cloud and aerosol layers along the satellite track are provided by the active instruments ATLID and CPR (e.g., van Zadelhoff et al., 2023; Donovan et al., 2023a; Kollias et al., 2023; Irbah et al., 2023). In order to get information about the scene around the satellite track, the passive imager MSI is necessary which provides columnar observations over a 150 km wide swath (Docter et al., 2023; Hünerbein et al., 2023b, a). The idea of combining the vertical information from

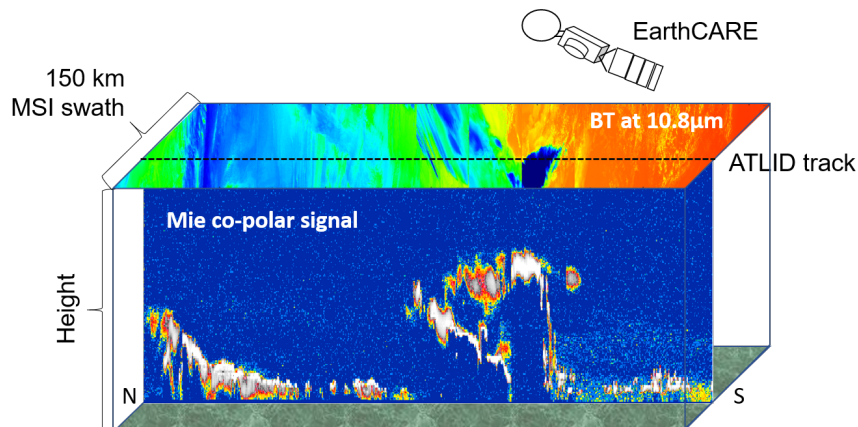


Figure 1. Combined view of ATLID ("curtain") and MSI ("carpet") on the simulated, so-called *Halifax* scene. A strong ATLID Mie co-polar signal (white color) indicates optically thick clouds, weaker signals (red to yellow) indicate optically thinner clouds or aerosol layer. The high clouds in the center of the scene are detected by MSI on the basis of their low brightness temperature (BT, blue color). The high brightness temperatures (red color) on the MSI swath result from the surface return where the low broken clouds are visible in yellow.

ATLID along track ("curtain") with the columnar information from MSI along and across track ("carpet") is illustrated in Fig. 1. This combination is an important step in the synergistic approach of EarthCARE, especially in estimating the cloud top height (CTH) of optically thin clouds and in assessing the aerosol type for the entire scene. The high-spectral-resolution lidar ATLID (do Carmo et al., 2021) operates at a wavelength of 355 nm with a vertical resolution of approximately 100 m below an altitude of 20 km and 500 m above 20 km. It provides vertical profiles along the satellite track of the particle backscatter and extinction coefficient, the lidar ratio, and the particle linear depolarization ratio which are **stored** in the ATLID L2a product A-EBD (ATLID Extinction, Backscatter, Depolarization, Donovan et al., 2023a). The multi-spectral imager MSI measures the radiances in the visible, near-infrared and infrared (central wavelengths: 0.67, 0.865, 1.65, 2.21, 8.8, 10.8, 12.0 μm) with a 500 m spatial resolution over a swath width of 150 km across track. Combinations of these wavelengths are used to derive a cloud mask which is provided in the MSI Cloud Mask product (M-CM, Hünnerbein et al., 2023b), and to retrieve cloud optical properties such as the cloud optical thickness (COT), CTH and the effective radius of the cloud droplets which **are** provided in the MSI Cloud Optical and Physical product (M-COP, Hünnerbein et al., 2023a). Aerosol products such as the aerosol optical thickness are retrieved for the cloud-free pixels and stored in the MSI Aerosol Optical Thickness product (M-AOT, Docter et al., 2023).

Regarding clouds, an accuracy of the CTH for ice and water clouds of 300 m is required (mission requirements) for a 3D scene. Such accuracy cannot be achieved with MSI retrievals alone. The MSI CTH retrieval (Hünnerbein et al., 2023a) is based on the measured radiation at 10.8 μm which is thermally emitted by clouds (Fritz and Winston, 1962; Smith and Platt, 1978; Wielicki and Coakley, 1981) and gives an infrared effective radiative height. The method provides reasonable estimates for the CTH for optically thick clouds, but in case of semi-transparent cloudiness the direct use of the measured brightness temperature will lead to a significant underestimation of the true CTH. On the other hand, ATLID can provide the physical boundaries of the cloud with the required accuracy (A-CTH product, Wandinger et al., 2023b), but only for an atmospheric cross section along track. Therefore, an algorithm for a synergistic ATLID–MSI CTH product (AM-CTH) is developed and described in the present paper. The AM-CTH product is based on the systematic investigation and classification of differences in the CTH obtained with ATLID and MSI along track. A scene classification scheme is developed to extrapolate the CTH difference to the MSI swath.

With respect to aerosol, the mission requirements demand to identify the presence of absorbing and non-absorbing aerosol particles from natural and anthropogenic sources. Vertically resolved aerosol typing is provided along track by the ATLID Target Classification (A-TC, Irbah et al., 2023). These aerosol types weighted by the extinction coefficient of the respective height level are integrated to a column aerosol mixture in the ATLID Aerosol Layer Descriptor (A-ALD, Wandinger et al., 2023b). **The M-AOT algorithm provides aerosol mixing ratios retrieved from MSI observations. The most robust way to compare the ATLID and MSI retrieved aerosol mixing ratios is the comparison of the dominant aerosol type, which is done in the ATLID–MSI Aerosol Column Descriptor (AM-ACD) algorithm. The Ångström exponent calculated from the ATLID observations at 355 nm and the MSI retrievals at wavelengths ≥ 670 nm (Docter et al., 2023) further constraints the aerosol typing because the spectral behavior contains information about the particle size.** The AM-ACD algorithm is developed as a synergistic product to combine aerosol information from the two instruments. The AM-ACD product contains

information on the spectral AOT, respective Ångström exponents, and an estimate of the aerosol type.

AM-COL extends the ATLID information over the entire swath as long as a swath pixel can be related to a track pixel. A more sophisticated approach including radiative transfer simulations is used for the pixels close to the track in the ACM-3D product (Qu et al., 2023). They prepare the data for the 100 km² snapshot (20 km along track × 5 km across track) which will be used for the radiative closure. These simulations can be done for two pixels in each direction from the track, but not for the entire swath. The AM-COL processor does not construct a 3D scene, but will provide the CTH and the columnar aerosol products (2D horizontally like a "carpet") for the entire MSI swath width of 150 km.

The paper is structured as follows. Sect. 2 provides an overview about previous efforts in combining active and passive remote sensing for the determination of the CTH and for aerosol typing. Then, a detailed description of the underlying AM-COL algorithms is provided in Sect. 3. The algorithm is validated using common test scenes from the EarthCARE End-to-End Simulator (Donovan et al., 2023b) in Sect. 4. Cloud and aerosol products are always treated separately. Major findings are summarized in the Conclusions.

2 Combining active and passive remote sensing

The combination of active and passive remote-sensing techniques onboard the EarthCARE satellite is essential to reach the mission goal of deriving the radiative flux at the top of the atmosphere with an accuracy of 10 Wm⁻² for a 100 km² snapshot view of the atmosphere. In this context, the accuracy of the CTH over the MSI swath as well as the imager-based aerosol typing needs some further discussion. This section intends to provide an overview about the current state of research of these two topics.

2.1 Improving passive CTH retrievals by active remote sensing

The CTH is detected from space by active and passive remote sensing. Passive retrievals use for example the MODerate-resolution Imaging Spectrometer (MODIS), the Spinning Enhanced Visible and InfraRed Imager (SEVIRI), **the TROPospheric Monitoring Instrument (TROPOMI, Loyola et al., 2018) on board the Sentinel-5 Precursor mission or in near future the Plankton, Aerosol, Cloud, ocean Ecosystem mission (PACE, Sayer et al., 2023)**. Active measurements are taken with lidars **as for example** from the Cloud-Aerosol Lidar and Infrared Pathfinder Satellite Observations (CALIPSO). Active remote sensing has a high vertical resolution in detecting the geometrical CTH, but is limited to observations along the narrow satellite track. Passive remote-sensing techniques offer a wider spatial coverage, but with limited vertical accuracy.

From the literature it is known that CTH retrievals from passive sensors can be highly erroneous. Comparisons with lidar measurements showed large discrepancies in dependence of the type, height, and optical thickness of the clouds. First space-borne comparisons of CTH detection with passive and active sensors were presented by Mahesh et al. (2004) and Naud et al. (2005). These authors used lidar observations from the Geoscience Laser Altimeter System (GLAS) to assess CTH accuracy for MODIS (aboard Terra and Aqua) and SEVIRI (aboard Meteosat-8). Beside discrepancies in the cloud mask, especially over polar regions and for optically thin clouds, they observed that the passive instruments overestimate the top height of low and

opaque clouds by 0.3–0.4 km and underestimate the CTH of high and optically thin clouds. Further comparison studies (Weisz et al., 2007; Holz et al., 2008; Minnis et al., 2008; Yao et al., 2013; Iwabuchi et al., 2016; Compernelle et al., 2021) reported different biases depending on geographical region, cloud type and altitude. Major improvements to the passive retrievals were achieved by MODIS Collection six (Baum et al., 2012). ESA’s Clouds Climate Change Initiative resulted in a comprehensive overview about state-of-the-art retrievals of cloud properties from passive sensors (Stengel et al., 2015). A very detailed study with wide spatial coverage was performed by Mitra et al. (2021). They investigated the bias of Terra-MODIS between 50°S and 50°N against the space lidar CATS (Yorks et al., 2016) for various altitude and cloud optical thickness (COT) ranges. In the case of high clouds (CTH > 5 km, defined by CATS), the bias (MODIS–CATS) was found to be –1.16 km (with a precision of 1.08 km), and for low clouds (< 5 km) the bias was 40 ± 730 m. Especially for low clouds, the bias strongly depends on COT: Optically thin (COT < 0.8) low clouds showed a negative bias of -440 ± 600 m, whereas optically thick (COT > 0.8) low clouds were found to have a positive bias of $+500 \pm 430$ m (Mitra et al., 2021). For high clouds, the bias reduces with increasing COT to –280 m for COT > 0.8. The presence of multi-layer clouds increases the bias between active and passive detection of CTH (-1.20 ± 1.19 km).

Special care has to be taken in presence of low-level clouds in the Arctic which under certain conditions are detected with an imager but not from a space lidar (Chan and Comiso, 2011). These clouds are frequently observed in summer (Griesche et al., 2020) and are hardly visible by ground-based cloud radars because of their low altitude. Further challenges for passive CTH detection occur in the presence of thick dust layers (e.g., Robbins et al., 2022). Thus, a proper aerosol–cloud discrimination is essential.

New algorithms use machine learning or neuronal networks to obtain the CTH from passive sensors (e.g., Håkansson et al., 2018; Min et al., 2020). These algorithms are trained on previous data sets using CALIPSO. As a recent example, Tan et al. (2022) published an algorithm to assess the CTH of overlapping clouds from the Advanced Himawari Imager (AHI). Their machine-learning approach uses the available information on cloud phase, COT and neighboring cloud pixels to estimate the CTH of water and overlaying ice clouds. In a validation against CloudSAT and CALIPSO the algorithm of Tan et al. (2022) led to a reduction of the mean CTH bias from –5.1 to –2.6 km.

2.2 Aerosol typing from combined active and passive remote sensing

Besides the knowledge about the aerosol optical thickness (AOT) and the aerosol layer heights, a correct aerosol typing is essential for radiative transfer calculations. The radiative properties of an aerosol layer depend on the aerosol type or mixture. In case of EarthCARE, the Hybrid End-To-End Aerosol Classification model (HETEAC, Wandinger et al., 2023a) is the underlying aerosol model linking the optical, microphysical and radiative properties of aerosol mixtures.

Aerosol classification schemes from active remote-sensing observations are based on the observed (intensive) optical properties. In the case of lidar measurements, the particle linear depolarization ratio (measure of particles’ non-sphericity) and the extinction-to-backscatter ratio (lidar ratio) are the main quantities used in aerosol classification schemes (e.g., Burton et al., 2012; Groß et al., 2015). A comprehensive data base of these intensive optical properties at 355 and 532 nm was collected by Floutsis et al. (2023). The CALIPSO aerosol classification scheme (Omar et al., 2009; Kim et al., 2018) could not use the

lidar ratio as input because there is no direct measurement of the extinction coefficient. In contrast to CALIPSO, EarthCARE will carry a high-spectral-resolution lidar (HSRL), which provides independent measurements of the particle extinction and backscatter coefficients (at 355 nm) and therefore enables an improved aerosol classification. The first HSRL system operated successfully in space was the lidar onboard of ESA's wind lidar mission Aeolus (Stoffelen et al., 2005) which enabled the independent measurement of the extinction coefficient (Ansmann et al., 2007; Flament et al., 2021). In the case of multi-wavelength observations, the Ångström exponent provides additional information about the particle size. A vertically-resolved aerosol typing is only possible with active remote-sensing instrumentation.

Passive remote-sensing techniques use multiple wavelengths to retrieve the AOT. From these AOT observations and the related Ångström exponents, the columnar aerosol type is determined (e.g., Toledano et al., 2007; Holzer-Popp et al., 2013; de Leeuw et al., 2015). Including polarization measurements (e.g., Russell et al., 2014) or trace-gas column densities (Penning de Vries et al., 2015) provides additional information to improve aerosol typing. In contrast to the Ångström exponent or the polarization, the AOT is an extensive property and therefore not intrinsic to a certain aerosol type.

3 ATLID–MSI Column Products processor (AM-COL)

The ATLID–MSI Column Products processor (AM-COL) produces the ATLID–MSI Cloud Top Height (AM-CTH) product and the ATLID–MSI Aerosol Column Descriptor (AM-ACD) product. These products belong to the EarthCARE L2b products defined in the ESA EarthCARE production model and product list (Wehr et al., 2023; Eisinger et al., 2023). Since their generation requires input from ATLID L2a products created in the ATLID Layer Products processor (A-LAY, Wandinger et al., 2023b) and MSI L2a products created in the MSI Cloud Products processor and the MSI Aerosol Optical Thickness processor (M-CLD and M-AOT, Hünerbein et al., 2023b, a; Docter et al., 2023), they are produced after the ATLID L2a and MSI L2a processing is completed. An overview about the main input and output parameters and the respective products in which they are contained is provided for the cloud products in Table 1 and for the aerosol products in Table 2.

All calculations within the AM-COL processor are performed for one grid cell horizontal resolution on the EarthCARE Joint Standard Grid (JSG). The A-LAY products (A-CTH and A-ALD) are already provided on JSG with this resolution (approximately 1 km) along track (see Table 1 and 2). The MSI products (M-CM, M-COP and M-AOT) are provided on the finer resolution of the MSI grid (500 m). Thus, a re-sampling is necessary, **which is illustrated in Fig. 2**. The surrounding nine MSI pixels correspond to one JSG pixel. A cloud fraction for each JSG pixel is calculated from the contributing MSI pixels. Only if all contributing MSI grid cells are categorized as cloud free (cloud fraction of 0%) or as cloudy (cloud fraction of 100%), the corresponding JSG pixel is set to cloud free or cloudy, respectively. The cloud mask for the MSI swath is provided in the M-CM product and it is based on threshold tests to brightness temperatures and reflectances of individual MSI channels (Hünerbein et al., 2023b).

The AM-COL processor is split in the cloud processing algorithm AM-CTH (Sect. 3.1) applied to all cloudy pixels and the aerosol processing algorithm AM-ACD (Sect. 3.2) applied to all cloud-free pixels. Aerosol layers above or below cloud layers

Table 1. The main input and output parameters for the ATLID–MSI Cloud Top Height product and the products in which they are contained (**bold, with references**). Dimensions: X – along track, Y – across track.

Product name	Resolution	Dimension
Input		
ATLID L2a Cloud Top Height (A-CTH, Wandinger et al., 2023b)		
– ATLID cloud top height	JSG	X
– Simplified uppermost cloud classification	JSG	X
MSI L2a Cloud Mask (M-CM, Hünerbein et al., 2023b)		
– MSI cloud mask	MSI grid	X,Y
– MSI cloud phase	MSI grid	X,Y
– Surface classification	MSI grid	X,Y
– M-CM quality status	MSI grid	X,Y
MSI L2a Cloud Optical and Physical products (M-COP, Hünerbein et al., 2023a)		
– MSI cloud top height	MSI grid	X,Y
– MSI cloud optical thickness	MSI grid	X,Y
– MSI cloud top pressure	MSI grid	X,Y
MSI L1c data		
– MSI brightness temperature at 10.8 μm	MSI grid	X,Y
– MSI brightness temperature at 12.0 μm	MSI grid	X,Y
– MSI reflectance at 0.67 μm	MSI grid	X,Y
Output		
ATLID–MSI L2b Cloud Top Height (AM-CTH, this paper)		
– ATLID–MSI cloud top height difference	JSG	X,Y
– MSI cloud top height	JSG	X,Y
– Cloud fraction	JSG	X,Y
– AM-CTH quality status	JSG	X,Y

are not considered.

3.1 ATLID–MSI Cloud Top Height (AM-CTH) algorithm

A flow chart for the ATLID–MSI Cloud Top Height (AM-CTH) algorithm is presented in Figure 3. It is applied to all JSG
180 pixels considered as cloud (cloud fraction of 100%) based on the MSI cloud mask. The main output of the AM-CTH processor is the CTH difference between ATLID and MSI. The ATLID CTH was determined using the wavelet covariance transform (WCT) method with thresholds from the ATLID Mie co-polar signal (Wandinger et al., 2023b). The MSI CTH provided in the M-COP product was retrieved from an optimal-estimation-based algorithm using the visible, near-infrared and thermal infrared

Table 2. The main input and output parameters for the ATLID–MSI Aerosol Column Descriptor product and the products (with references) in which they are contained. Dimensions: X – along track, Y – across track, C₄ – MSI aerosol components, C₇ – ATLID aerosol types

Parameter	Resolution	Dimension
Input		
ATLID L2a Aerosol Layer Descriptor (A-ALD, Wandinger et al., 2023b)		
– Column aerosol optical thickness at 355 nm	JSG	X
– Columnar aerosol classification probabilities	JSG	X,C ₇
– Number of detected aerosol layers	JSG	X
MSI L2a Aerosol Optical Thickness (M-AOT, Docter et al., 2023)		
– Column aerosol optical thickness at 670 nm	MSI grid	X,Y
– Column aerosol optical thickness at 865 nm	MSI grid	X,Y
– Aerosol component mixing ratios	MSI grid	X,Y,C ₄
– Homogeneity flag	MSI grid	X,Y
– M-AOT quality status	MSI grid	X,Y
Output		
ATLID–MSI L2b Aerosol Column Descriptor (AM-ACD, this paper)		
– Ångström exponent (355 nm /670 nm, 670 nm/865 nm)	JSG	X,Y
– Aerosol optical thickness at 355/670/865 nm	JSG	X,Y
– Dominant aerosol type	JSG	X,Y
– Dominant aerosol type flag	JSG	X,Y
– AM-ACD quality status	JSG	X,Y

MSI measurements (Hünerbein et al., 2023a).

185 In a first step, the synergistic ATLID–MSI CTH difference along track is calculated. Then, the scene on the MSI swath has to be classified in order to find similar cloud conditions as along the track. The scene is classified with further input from the M-COP and M-CM products (e.g., COT and cloud phase) and from the MSI L1c data such as the reflectance at 0.67 μm and the brightness temperatures at 10.8 and 12.0 μm. Multi-layer cloud scenarios are searched in an extra step. Then, the CTH difference is transferred to the MSI swath. The similarity between a pixel on the swath to an along-track pixel is used
190 to assign the same CTH difference to the across-track pixel. At the end, the quality status of the product is determined (see Appendix A1).

The difference of the ATLID CTH and the MSI CTH is calculated along track (ATLID minus MSI). The CTH difference found on the track is related to the swath pixels under consideration of five criteria which are based on the previous scene classification:

- 195
1. Agreement in cloud type (ISCCP plus multi-layer class)
 2. Agreement in cloud phase (water, ice, supercooled mixed-phase, multi-layer cloud)

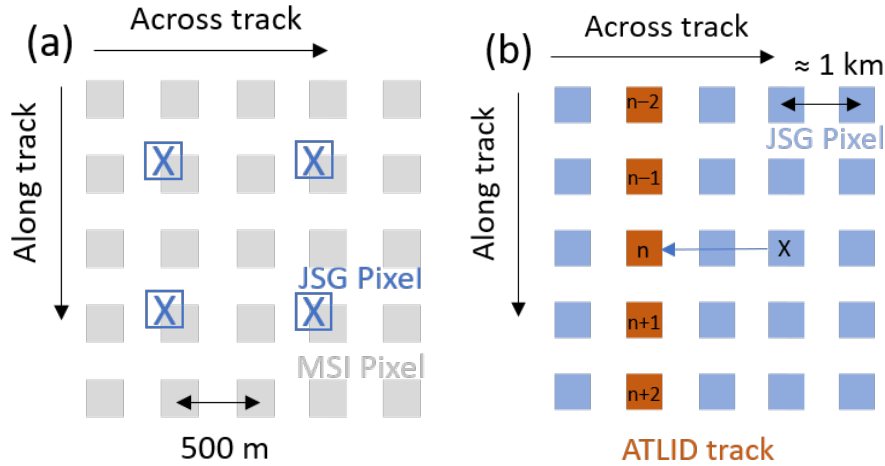


Figure 2. (a) The sketch illustrates the mapping of the MSI grid to JSG. A nearest neighbor search is implemented to link a JSG pixel to the closest MSI pixel. Usually, 9 MSI pixels correspond to one JSG pixel. (b) The sketch illustrates the transfer of the CTH difference from the track to the swath. For an across-track pixel, first the nearest along-track is compared (5 or 3 criteria, see Fig. 3). If no agreement was found, the search continues alternating North ($n-1$) and South ($n+1$) of the closest along-track pixel until agreement is found or a configurable maximum search distance is reached. Then, the process is repeated for the next across-track pixel.

3. Agreement in surface type (water, land, desert, vegetation, snow, sea ice, sun glint)
4. **Satisfaction of the criterion in** brightness temperature ($10.8 \mu\text{m}$) difference threshold (**Equation 1**)
5. **Satisfaction of the criterion in** reflectivity ($0.67 \mu\text{m}$) difference threshold (**Equation 2**)

200 The cloud phase and surface type are provided in the M-CM product. The AM-CTH algorithm transfers them to JSG resolution under the condition that all contributing MSI pixels must have the **same cloud phase or surface type, respectively**.

In order to transfer the difference detected along track to the entire MSI swath, the cloud type of each JSG pixel has to be determined. The nine cloud classes (cumulus, altocumulus, cirrus, stratocumulus, altostratus, cirrostratus, stratus, nimbostratus, deep convection) defined by the International Satellite Cloud Climatology Project (ISCCP classes, Rossow and Schiffer, 1999) are used to categorize the cloud type of each JSG pixel. ISCCP categorizes the cloud classes by means of the cloud top pressure and the COT. From the MSI pixels contributing to one JSG pixel, the lowest cloud top pressure and the corresponding COT are used as input for classifying the JSG pixel. Both quantities are provided in the M-COP product (Table 1). Additionally, a tenth cloud class is defined as the multi-layer class. For the identification of multi-layer cloud scenarios on the MSI swath we adapt a method developed by Pavolonis and Heidinger (2004), which was used in M-CLD as well (Hünerbein et al., 2023b). It makes use of the visible reflectance (at 670 nm) and the MSI brightness temperatures at 10.8 and $12.0 \mu\text{m}$ ($T_{10.8}$ and $T_{12.0}$). Pavolonis and Heidinger (2004) simulated brightness temperature difference ($T_{10.8} - T_{12.0}$) as function of the reflectance in

210

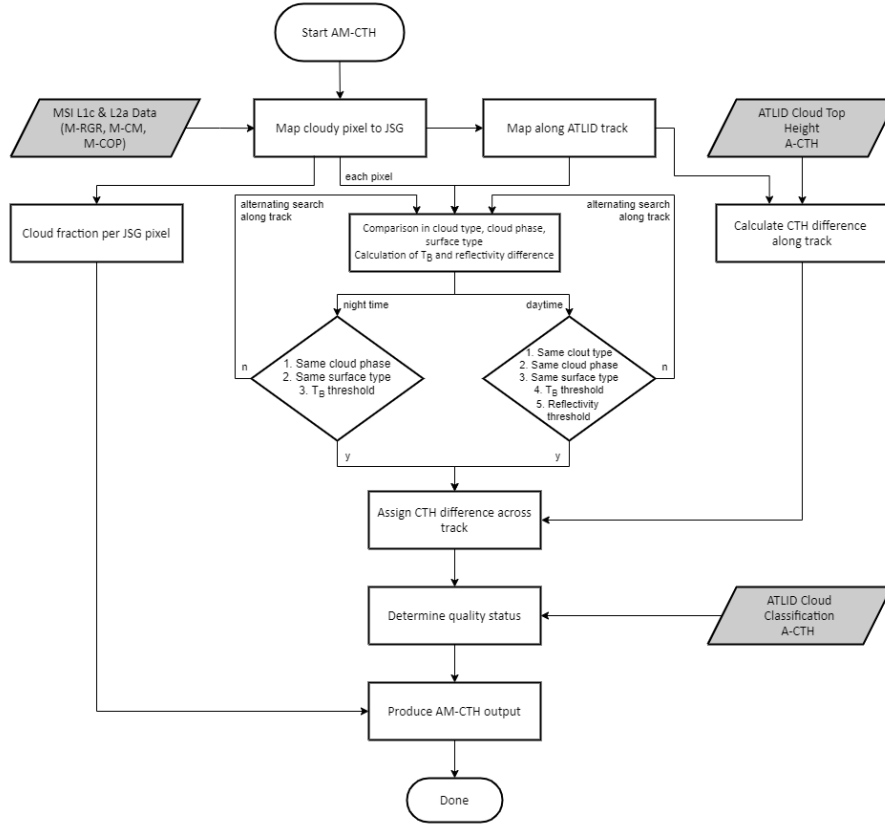


Figure 3. Flow chart of the ATLID–MSI Cloud Top Height (AM-CTH) algorithm. The algorithm is applied to all cloudy JSG pixels. T_B stands for brightness temperature at $10.8 \mu\text{m}$.

order to set a threshold for the multi-layer-cloud detection. The combined ATLID and MSI observations along the satellite track will create an unique dataset to derive this threshold from observations. Along the ATLID track, the vertical information of ATLID easily reveals multi-layer cloud scenarios (for a semi-transparent upper cloud layer) which are flagged in the simplified uppermost cloud classification of the A-CTH product. There, multi-layer clouds are defined when a configurable number of pixels between two detected cloud layers are cloud free (default 5 pixels, corresponding to 500 m).

Besides the agreement in cloud type, cloud phase, and surface type, two homogeneity criteria are used to determine whether the measured swath pixel can be related to a track pixel. The first criterion is based on a threshold ($\Delta T_{\text{th},10.8}$) for the difference of the brightness temperature at $10.8 \mu\text{m}$ ($T_{10.8}$) between swath (s) and track pixels (t):

$$|T_{10.8,t} - T_{10.8,s}| < \Delta T_{\text{th},10.8}. \quad (1)$$

The second criterion uses a threshold ($\Delta\rho_{\text{th},0.67}$) for the difference of the MSI reflectance $\rho_{0.67}$ at 0.67 μm between swath (s) and track (t) pixels:

$$|\rho_{0.67,t} - \rho_{0.67,s}| < \Delta\rho_{\text{th},0.67}. \quad (2)$$

The thresholds are configurable. The default values are $\Delta T_{\text{th},10.8} = 10 \text{ K}$ and $\Delta\rho_{\text{th},0.67} = 0.1$ based on tests with the simulated EarthCARE test scenes (see Sect. 4).

At daytime conditions, all five criteria are used to relate a swath pixel to a track pixel. Without sunlight, there is no measurement of the reflectance at 0.67 μm , and the **M-COP** algorithm cannot determine the COT and thus the cloud type. Thus, at nighttime, only three criteria (brightness temperature difference at 10.8 μm and agreement in cloud phase and surface type) are used. The quality status is set accordingly (see Appendix A1).

The search for agreement is illustrated in Figure 2. It starts at the closest along-track pixel and continues by searching one pixel before (e.g., to the North) and one pixel after (e.g., to the South) from the closest pixel along track. This alternating search is continued until an agreement is found or the configurable maximum search distance is reached (default 75 **JSG pixels (approximately 75 km)** in each direction along track). If a measurement at swath fits to an along-track measurement for all criteria, then the observed CTH difference from the track is assigned to the swath pixel. **Otherwise, no CTH difference is assigned to the pixel.**

3.2 ATLID–MSI Aerosol Column Descriptor (AM-ACD) algorithm

The structure of the ATLID–MSI Aerosol Column Descriptor (AM-ACD) algorithm is illustrated in Figure 4. The algorithm is applied to all JSG pixels with a cloud fraction of 0%. The AM-ACD product contains information on the columnar aerosol optical properties. It provides the spectral aerosol optical thickness (AOT, 355 and 670 nm over land and 355, 670 and 865 nm over ocean), the respective Ångström exponents and their uncertainties (see Table 2).

In the first step, ATLID and MSI collocated aerosol type information along track are compared (Sect. 3.2.1) and the Ångström exponent (355 nm/ 670 nm) is calculated. The ATLID AOT at 355 nm is spread over the swath in case the dominant aerosol type agrees between swath and track (Sect. 3.2.2). By investigating the horizontal homogeneity of the MSI AOT at 670 nm (identification of aerosol plumes), the ATLID aerosol typing can be spread over the entire swath or parts of it (Sect. 3.2.3). The product contains a quality indicator which considers information on aerosol layering provided by A-ALD and an overall quality status of the product (see Appendix A2).

3.2.1 Comparison of the dominant aerosol type

In Section 2.2 the active and passive aerosol typing approaches were introduced. The ATLID aerosol typing is based on the measurements of the linear depolarization ratio and the lidar ratio. **Six aerosol types (dust, marine aerosol, continental pollution, smoke, dusty smoke, dusty aerosol mix) and ice are distinguished in the A-TC product (Irbah et al., 2023).** The ice is considered to indicate the presence of optically thin ice-containing layers (e.g., diamond dust, subvisible cirrus) that have not been identified as clouds and thus occur in the aerosol products (Irbah et al., 2023; Wandinger

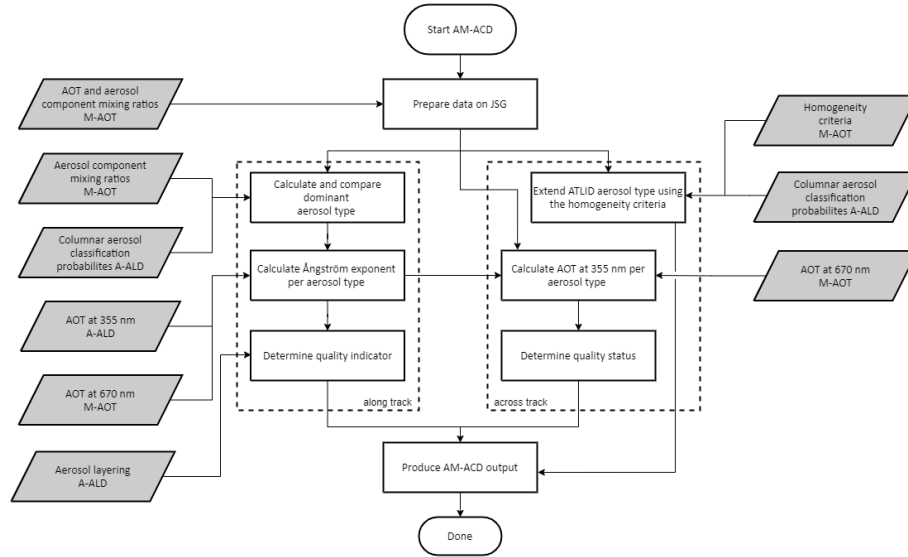


Figure 4. Flow chart of the ATLID–MSI Aerosol Column Descriptor (AM-ACD) algorithm. The algorithm is applied to all cloud-free JSG pixels.

et al., 2023b). If the aerosol type ice amounts to a significant contribution ($> 20\%$ in terms of AOT, configurable) of the column integrated aerosol classification, a cirrus cloud is included in the profile which was not detected by the A-CTH algorithm. The profile is therefore not cloud free and a warning is raised (see quality status in Appendix A2). In the following, only the six aerosol types (excluding the ice) are considered for comparison between ATLID and MSI aerosol classifications. The aerosol types are provided as a vertical profile in the A-TC product and used by the A-ALD algorithm to calculate the column-integrated aerosol classification probabilities for a better comparison with MSI.

The MSI aerosol typing is based on an a priori aerosol climatology over land taken from Kinne et al. (2013) and on a best fitting component mixture to the MSI measurements over ocean (Docker et al., 2023). The M-AOT aerosol classification uses 25 mixtures of the four aerosol components defined by HETEAC (see Table 2 in Docker et al. (2023)). The four HETEAC aerosol components include two fine modes (weakly absorbing and strongly absorbing) and two coarse modes (spherical and non-spherical) as described in Wandinger et al. (2023a).

The dominant aerosol type is defined by the highest columnar aerosol classification probability (A-ALD product). In Table 3, the six A-TC aerosol types are expressed in terms of the four HETEAC aerosol components which are used in M-AOT. The first four A-TC types (dust, marine aerosol, continental pollution, smoke) are clearly dominated by one the four HETEAC components even if other aerosol components contribute to these types. The A-TC aerosol types dusty smoke and dusty aerosol mix are a mixture of two or three HETEAC aerosol components. Both mixtures are found for an AOT contribution of coarse-mode non-spherical (CMNS) aerosol between 25 and 50%. The more absorbing dusty smoke requires more than 20% of fine-mode strongly absorbing (FMSA) aerosol; whereas the less absorbing dusty aerosol mix should have a

contribution of less than 20% of fine-mode strongly absorbing aerosol.

Along the ATLID track a direct comparison of the six A-TC aerosol types and the four HETEAC components **which mixing is provided by M-AOT** is achieved. If A-TC is dominated by a mixture (dusty smoke or dusty aerosol mix), the above derived thresholds are applied for the comparison with the M-AOT aerosol classification. In case of agreement, the dominant aerosol type flag is set to 1, otherwise it is 0.

Table 3. The representation of the six aerosol types from the ATLID target classification (A-TC, Irbah et al., 2023) in terms of AOT contributions of the four basic aerosol components defined in HETEAC (Wandinger et al., 2023a) **which are used in M-AOT**: FMWA – fine mode weakly absorbing, FMSA – fine mode strongly absorbing, CMS – coarse mode spherical and CMNS – coarse mode non-spherical. The optical properties (particle linear depolarization ratio and the lidar ratio at 355 nm) and uncertainty ranges are provided for each A-TC aerosol type.

A-TC aerosol type	Optical properties		AOT contribution (in %)			
	Depol. ratio	Lidar ratio (sr)	FMWA	FMSA	CMS	CMNS
Dust	0.22±0.05	55±15	14	0	2	85
Marine aerosol	0.03±0.04	20±12	0	0	99	1
Cont. Pollution	0.03±0.04	55±15	85	0	12	2
Smoke	0.03±0.04	88±12	22	76	0	2
Dusty smoke	0.14±0.06	73±15	0	61	0	39
Dusty aerosol mix	0.14±0.06	43±15	36	0	26	38

275

3.2.2 Extrapolation of the AOT at 355 nm from the track to the swath

The idea of the AM-ACD algorithm is to extrapolate the AOT at 355 nm as measured with ATLID to the MSI swath in order to increase the aerosol information over the entire swath. Therefore, it is important to capture the spatial extent of an aerosol plume across track and combine it with the measurements along track. ATLID observes the AOT at 355 nm, MSI at 670 and 865 nm over ocean and at 670 nm over land. The Ångström exponent describes the spectral AOT behavior. It is an aerosol-type characteristic parameter which mainly contains information on the mean size of the particles (e.g., Toledano et al., 2007). If the dominant aerosol type agrees (see Sect. 3.2.1), the AM-ACD algorithm calculates the Ångström exponent (355 nm/670 nm) along track. In every EarthCARE frame (1/8 orbit) the mean Ångström exponent is calculated per dominant aerosol type (if it is present within the frame). From the MSI aerosol classification the dominant aerosol type is derived for each JSG pixel across track. In case the same dominant aerosol type was detected along track as well, the respective Ångström exponent is used to calculate the AOT at 355 nm from the MSI-measured AOT at 670 nm. An aerosol plume consisting of a dominant aerosol type which is just present on the MSI swath but not on the ATLID track cannot be handled by the AM-ACD algorithm as the information about the relationship between the two wavelengths is missing.

Alternatively, HETEAC could be used to calculate the Ångström exponent based on the aerosol component mixing ratios

290 (from M-AOT) or the columnar aerosol classification probabilities (from A-TC, A-ALD). However, we decided to implement the described observation-driven approach in AM-ACD.

3.2.3 Extension of the ATLID aerosol classification to the MSI swath

The M-AOT product provides a homogeneity flag (Table 2) which indicates whether the optical properties of the surrounding pixels are counted as homogeneous. This flag is used to transfer the dominant aerosol type derived from ATLID observations
295 along track to the MSI swath. As long as the homogeneity criterion is fulfilled the same dominant aerosol type as derived for the closest along-track pixel could be assumed for the across-track pixel. The additional M-AOT aerosol typing provides the possibility of comparison.

A simple aerosol classification based on the AOT at 670 nm and the Ångström exponent (355 nm/670 nm) would be possible. Passive remote-sensing techniques applied this method in the past (e.g., Toledano et al., 2007). However, we do not consider
300 the AOT as an adequate parameter for aerosol typing because it depends on the amount of aerosol (extensive quantity) and not on the aerosol type characteristics. As an example, a thin dust layer (low AOT, low Ångström exponent) might be misclassified as marine aerosol. Here, we prefer to extend the ATLID aerosol typing to the swath. It is based on the intensive quantities of particle linear depolarization ratio and lidar ratio. To stay with the example, the higher depolarization ratio would clearly identify the dust layer and would not lead to a confusion with marine aerosol. We leave it open to the user to construct an own
305 aerosol classification scheme based on the columnar quantities provided (AOT at 355, 670 nm and over ocean additionally at 865 nm and the respective Ångström exponents, see Table 2).

4 Validation of the AM-COL processor with the EarthCARE test scenes

The synergistic AM-COL processor does only partly use L1 data from instruments but mainly combines ATLID and MSI L2a products to generate a L2b columnar product. This fact prevents us from using real-world data for its validation. As presented
310 in Section 2.1, MODIS-retrieved CTHs are validated against space-lidar derived CTHs. The synergistic AM-COL processor already combines active and passive remote sensing. Thus, at the present state it can be only validated against simulated test scenes available for the EarthCARE processing chain.

And more specifically with the EarthCARE End-to-End Simulator specific test scenes **which** were created to test the full chain of EarthCARE processors (Donovan et al., 2023b). All scenes are based on the Global Environmental Multiscale (GEM) model
315 output (Qu et al., 2022). The aerosol fields are taken from the Copernicus Atmosphere Monitoring Service (CAMS) model. In the following, we present results obtained with the AM-COL processor for the so-called *Halifax*, *Hawaii* and *Halifax aerosol* scene. A detailed description is presented in Donovan et al. (2023b), **especially in Sections 3.1, 3.3 and 3.4. Furthermore, we want to refer to the plots of the ATLID Mie co-polar signal and the CTH in Wandinger et al. (2023b), there the *Halifax* scene is shown in Figure 6 and the *Halifax aerosol* scene in Figure 9.**

320

4.1 AM-CTH validation

Firstly, the output of the AM-CTH algorithm is presented (Sect. 4.1.1). Then, the output is validated against the GEM model truth (Sect. 4.1.2) with a special discussion on cloud class and multi-layer clouds (Sect. 4.1.3).

4.1.1 AM-CTH output for the *Halifax* scene

325 The validation of the AM-CTH product is shown for the *Halifax* scene. In a first step, we compute the CTH difference (ATLID – MSI) for all cloudy JSG pixels along the ATLID track. In Figure 5, the CTH of A-CTH and M-COP are shown together with the CTH difference (AM-CTH) for the *Halifax* scene along the ATLID track. **The CTH difference is small for the scattered clouds in the South ($< 32^\circ\text{N}$) and for the optically thick cirrus cloud at $36\text{--}39^\circ\text{N}$. However, the multi-layer cloud scenario in the center ($39\text{--}47^\circ\text{N}$) leads to large differences. MSI is sensitive to the optically thick liquid-containing clouds at $5\text{--}7\text{ km}$ height and ATLID detects the thin cirrus cloud at 11 km height as CTH. Further north ($>50^\circ\text{N}$), night-time conditions limit the abilities of MSI to detect the CTH. Nevertheless, the agreement is mostly within 2 km , except for the high clouds north of 65°N .**

Figure 6 presents the five quantities needed to transfer the CTH difference from the track to the swath. The reflec-

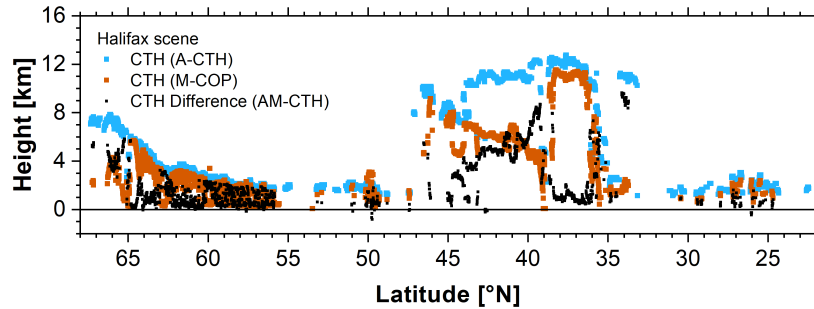


Figure 5. CTH along the ATLID track derived by ATLID (blue dots) and MSI (orange dots). AM-CTH calculates the difference (black dots) to transfer it to the MSI swath. The results are shown for the *Halifax* scene. **More details concerning the ATLID CTH are shown in Fig. 6. of Wandinger et al. (2023b).**

335 tivity (Fig. 6e) cannot be measured at night time and the cloud type (Fig. 6a) is not retrieved for night-time or twilight conditions ($>50^\circ\text{N}$). Then, only the remaining 3 criteria can be applied. During night-time, the cloud phase retrieval (Fig. 6b) alternates between ice and supercooled mixed phase clouds. Only, if all contributing MSI pixel show the same cloud phase, a cloud phase value is assigned to the JSG pixel. Otherwise no CTH difference is not transferred for the JSG pixel. It results in white spots in Figure 7b and decreased quality status. The brightness temperature at $10.8\text{ }\mu\text{m}$ (Fig. 6d) provides information about the scene at day and night and is therefore a valuable input parameter. The surface (Fig. 6c) does not depend on the cloud properties. The criterion of the same surface is rather conservative to be sure

340 that only similar MSI pixels are used for the track-to-swath method.

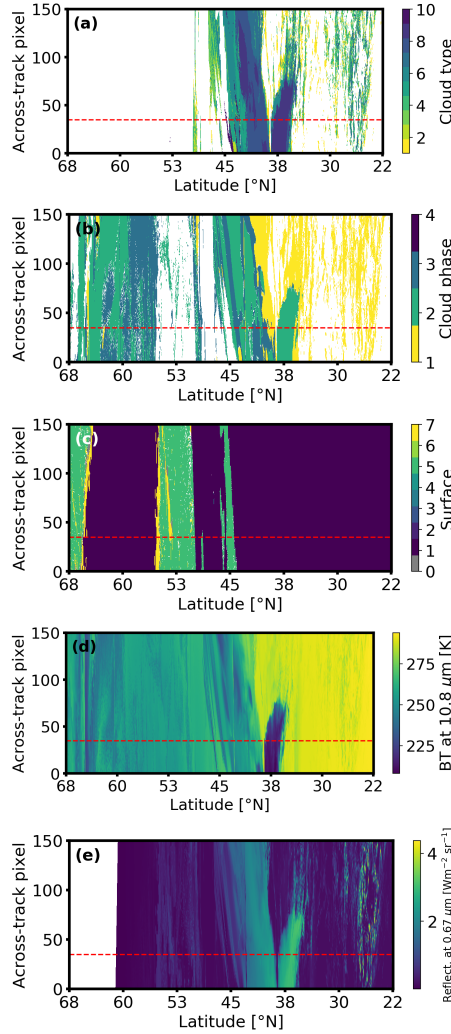


Figure 6. MSI input for the *Halifax* scene on JSG. (a) Cloud type defined by ISCCP and multi-layer class. (b) Cloud phase: 1 – water, 2 – ice, 3 – supercooled mixed-phase, 4 – multi-layer clouds. (c) Surface type: 1 – water, 2 – land, 3 – desert, 4 – vegetation, 5,6 – snow, 7 – sea ice (detailed description in Hünérbein et al. (2023b)). (d) Brightness temperature at 10.8 μm . (e) Reflectivity at 0.67 μm . The ATLID track is marked with a red dashed line.

Fig. 7 shows the MSI-derived CTH (on JSG), the synergistic ATLID–MSI CTH difference and the AM-CTH quality status. North of 50°N, no sunlight is present (nighttime observations) leading to limitations in the **M-COP** retrieval which are accounted for in the quality status (Fig. 7c). **The quality status is 3 (or worse).** Here, only three out the five criteria for the track-to-swath transfer could be applied. Cloud-free parts are shown in black for the AM-CTH products. The CTH difference is color-plotted over the cloudy parts shown in white. AM-CTH can provide a CTH for half of the cloudy JSG pixels (51%) defined by MSI. There are several reasons **why a CTH difference can not be transferred from the track to the swath**: (1)

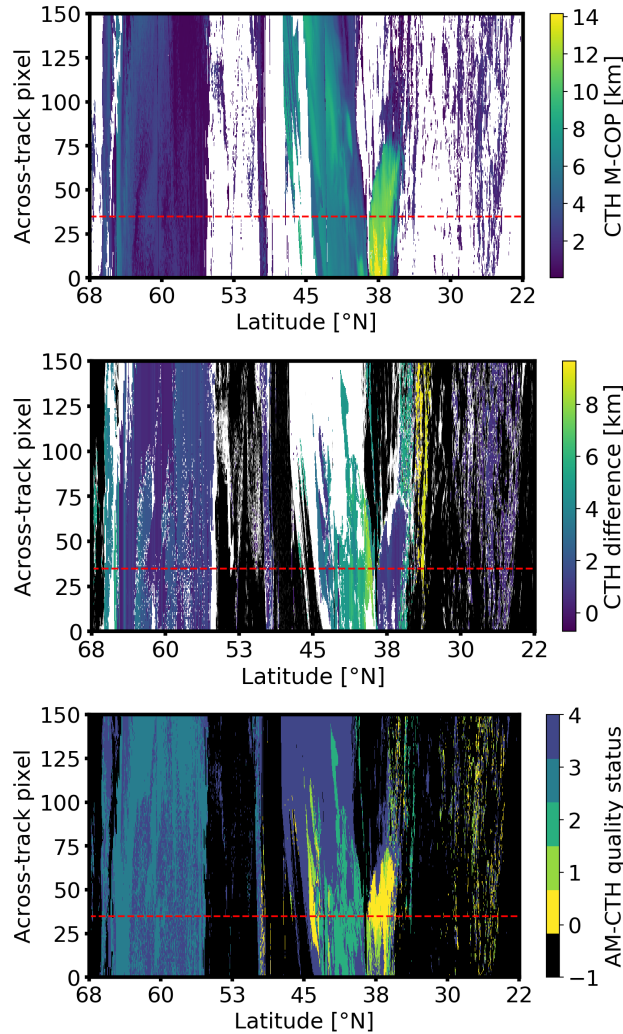


Figure 7. CTH for the *Halifax* scene as detected with MSI (M-COP algorithm) on JSG (top) and the synergistic ATLID–MSI CTH difference (AM-CTH product, center). Black areas are cloud free. In the white areas M-CM detected a cloud which was not transferred by AM-CTH. The quality status of the AM-CTH product (bottom) ranging from 0 (high quality) to 4 (bad quality). A quality status of -1 is given to (cloud-free) pixels for which the AM-CTH was not applied. The ATLID track is marked with a red dashed line.

The field of high cirrus clouds in the center could not be transferred for the entire swath. For the across-track pixels > 60 , no along-track pixels agreeing in all five criteria could be found within ± 75 pixels in each direction to transfer the CTH difference. **Even a larger search distance would only slightly increase the number of agreeing across-track pixels.** (2) During the nighttime observations ($> 50^\circ\text{N}$) the limited information from M-COP and a quickly changing cloud phase (one of the three nighttime criteria) made a transfer of the synergistic CTH difference difficult. **(3) A changing surface below the scene further limits the possible along track pixels to transfer the CTH difference (see Fig. 6c).**

The large CTH differences in the center of the scene are originating from the thin cirrus above the liquid-containing clouds as seen already in the CTH difference along track (Fig. 5). The large CTH difference around 34°N is probably a misinterpretation of **the AM-CTH algorithm** due to a thin cirrus which was present along track above the low clouds. The CTH difference is small (< 2 km) in the case of the mixed-phase clouds north of 55°N, the optically thick cirrus in the center and the shallow marine cumulus clouds in the South of the scene. The algorithm performance **is compared against the model truth in the following subsection. Then**, different cloud types are studied in more detail in Sect. 4.1.3.

360 4.1.2 CTH validation against the model truth

The results of the AM-CTH algorithm are validated against the GEM model truth (Qu et al., 2022; Donovan et al., 2023b). In the model, the extinction coefficients for cloud water and cloud ice are provided. The central question is: How to define the CTH from the true cloud extinction fields? Here, we will follow two distinct approaches: an extinction threshold and a cloud optical thickness (COT) threshold.

365 The ATLID-based approach as followed in A-CTH validation (Wandinger et al., 2023b) uses an extinction threshold. The CTH is defined when the cloud extinction reaches for the first time (coming from above) a certain threshold value. In the A-CTH validation an extinction threshold of 20 Mm^{-1} provided reasonable agreement between ATLID CTH and the model truth (Wandinger et al., 2023b). It provides an indication about the sensitivity of the A-CTH algorithm in detecting CTHs. This method defines the cloud as a geometrical feature and is sensitive to optically thin and thick clouds.

370 The MSI-based approach as followed in M-CLD validation (Hünerbein et al., 2023a, b) uses a COT threshold approach. Coming from above the extinction coefficient is integrated till a certain threshold COT is reached. Here, a COT threshold of 0.25 is used following the investigations of Stengel et al. (2015). They applied this threshold to CALIPSO-derived CTHs to get a better agreement with CTHs derived from passive imagers considering the different capabilities in CTH detection. This method defines the cloud as radiative feature and is rather sensitive to optically thicker clouds.

375 Both methods to derive the true CTH from the GEM model truth are compared in Fig. 8. The results are shown for the 364 k (kilo – 10^3) cloudy JSG pixels detected by the MSI cloud mask in the *Halifax* scene. The validation of the MSI cloud mask against the model truth is discussed in Hünerbein et al. (2023b). In the validation of AM-CTH, we are limited to the clouds detected by M-CM on the MSI swath. From the scatter plot, it can be clearly seen that the CTH defined by an extinction threshold of 20 Mm^{-1} is always equal or higher compared to the COT threshold of 0.25. However, in 65% of the cloudy pixels
380 the CTH agrees within $\pm 300 \text{ m}$. Especially the high clouds (>10 km height) are optically thin and reach the COT threshold of 0.25 at a lower altitude. For the validation against the model truth, we follow both CTH definitions as the best solution depends on the research interests of the users.

The validation with the extinction threshold is shown in Fig. 9 for the MSI-alone and the ATLID–MSI retrieval as histogram and scatter plot. **M-COP** provides a CTH for 350 k JSG pixels (96%) out of the 364 k pixels detected as cloudy by the MSI
385 cloud mask due to further quality checks in the M-COP algorithm. The AM-CTH algorithm could not assign a CTH difference for every cloud found by M-CM because several homogeneity criteria (see Sect. 3.1) have to be fulfilled to confidently translate a CTH difference from the track to the swath. Just for half of the CTHs (**177 k**, 51%) provided in M-COP, AM-CTH can provide

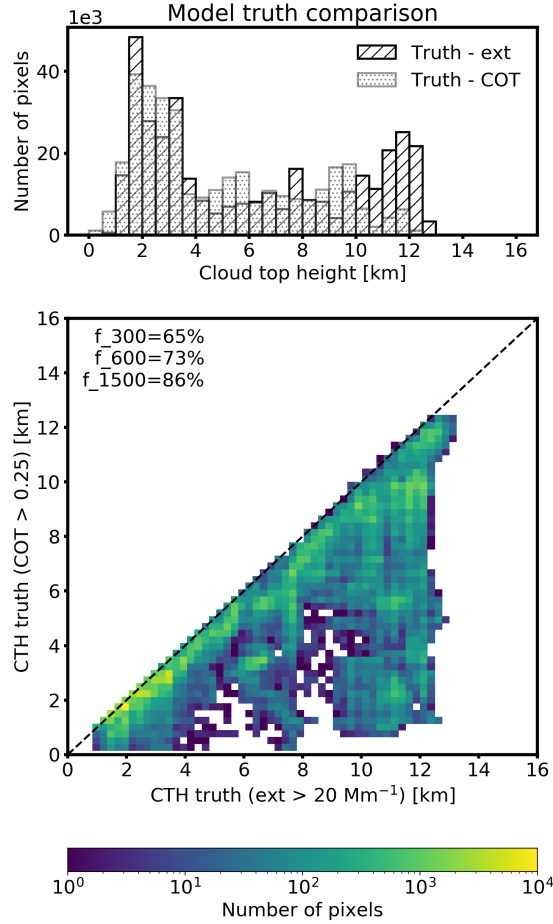


Figure 8. Comparison of the true CTH from GEM model output for the *Halifax* scene derived via an extinction threshold of 20 Mm^{-1} (hatched) and a COT threshold of 0.25 (dotted) for all 364 kilo (factor 10^3) JSG pixels with a cloud fraction of 100%. The indicator f_i displays the percentage of data points within $\pm i$ m from the 1:1 line. The scatter plot shows that the CTH based on the extinction threshold is always higher compared to the COT threshold.

a CTH. In case of AM-CTH, 63% of the detected CTH are within ± 600 m from the 1:1 line. 40% are within ± 300 m which was defined in the mission requirements. Some cirrus clouds on the swath are not detected and thus the CTH is underestimated.

390 In some other cases, AM-CTH transferred a high (cirrus) CTH to the swath, although there were only low clouds present. Both issues occur on the swath, there just the MSI information is present. In the majority of the cases, AM-CTH captured the (geometric) CTH. The MSI stand-alone retrieval tends to underestimate the (geometric) CTH, especially for the high clouds and some of the low clouds (see further cloud-type separated discussion in Sect. 4.1.3). Still 22% of the detected CTH are within ± 600 m from the 1:1 line.

395 The picture changes when considering the COT-based threshold for defining the true CTH (Fig. 10). There, M-COP shows a much better agreement, because the threshold is less sensitive to the thin cirrus clouds and represents the radiative CTH (Stengel et al., 2015). Now, 53% of the **M-COP** CTHs fall within ± 600 m of the 1:1 line. AM-CTH overestimates the (radiative) CTH showing a positive bias to the 1:1 line (37% within ± 600 m). Especially the cirrus clouds between 9 and 13 km height are detected by AM-CTH **below** a COT of 0.25.

400 The amount of data points within an interval of $\pm i$ m around the 1:1 line (f_i in Fig. 9 and 10) shows a similar behavior for **AM-CTH** to extinction-based model truth (40, 63, 82% for 300, 600, 1500 m) and **M-COP** to COT-based model truth (31, 53, 77% for 300, 600, 1500 m). This behavior underlines the finding that the extinction-based geometric CTH is detected by **AM-CTH** and the COT-based radiative CTH is detected by **M-COP**. In the following, we follow the extinction threshold defined CTH. A separation per ISCCP cloud type is provided in Section 4.1.3. There, a special focus is put on the multi-layer

405 cloud scenarios.

4.1.3 AM-CTH algorithm performance for different cloud classes

The performance of the AM-CTH algorithm was tested for the nine ISCCP cloud classes (Rossow and Schiffer, 1999) and the multi-layer class. The detection of the latter one is mainly based on the work by Pavolonis and Heidinger (2004). **However, the brightness temperature difference between 10.8 and 12.0 μm was not sensitively enough simulated in the EarthCARE**

410 **test scenes to clearly detect multi-layer clouds with MSI.** Fig. 11 presents the histograms of the CTH detected by M-COP (orange), the synergistic CTH by AM-CTH (red) and the true CTH (hatched) from the GEM model based on an extinction threshold of 20 Mm^{-1} for all clouds detected by the MSI cloud mask in the *Halifax* scene. In Figure 11, the cloud class for each JSG pixel was determined by the GEM model output (**CTH determined with an extinction threshold of 20 Mm^{-1} and COT) only for the pixels detected as cloudy by M-CM.** The corresponding M-COP and AM-CTH results are sorted

415 in the same cloud-class category. Best agreement between M-COP and the model truth is reached for stratus, nimbostratus and stratocumulus clouds which are optically thick. AM-CTH is based on M-COP and thus agrees well with the model truth for these cloud classes. The AM-CTH algorithm improves the (geometric) CTH detection compared to M-COP in two areas: (1) high clouds which are underestimated by M-COP as they are too thin to be detected with MSI; and (2) cumulus and altocumulus clouds for which the CTH is detected too low by MSI. A closer inspection of the vertical profiles of the extinction

420 in each cloud class showed that the maximum in the extinction and thus optical depth is reached much lower than the geometric CTH, especially for the optically thin clouds (left column of Fig. 11) and the high clouds (top row of Fig. 11). In general, MSI underestimates the CTH if we consider the geometric boundaries of the cloud by applying an extinction-based threshold (Fig. 9 and 11). MSI is sensitive to the radiative boundary of the cloud (see COT-based threshold in Fig. 10), which coincides with the

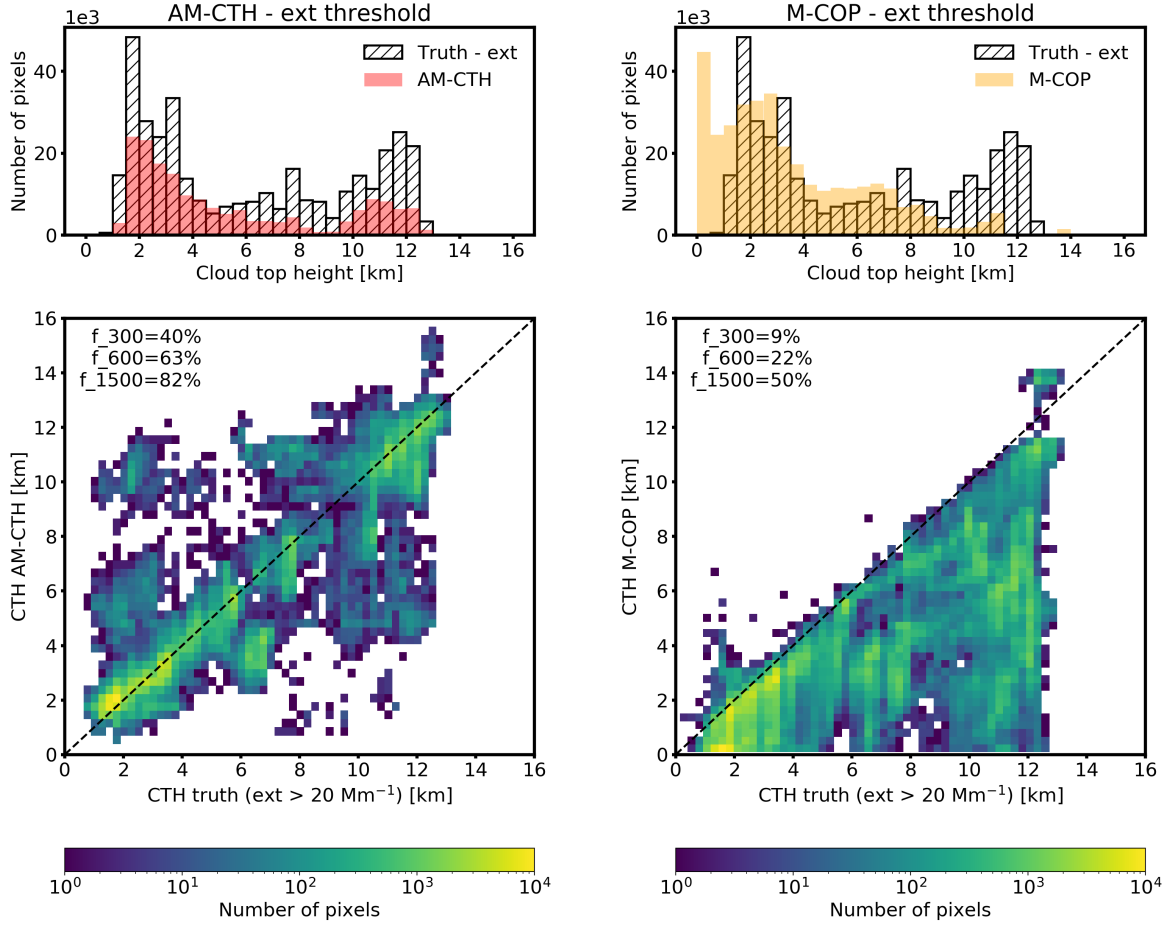


Figure 9. CTH validation against the GEM model truth for the *Halifax* scene. The true CTH was determined by the ATLID-based definition with a cloud extinction threshold of 20 Mm^{-1} for all cloudy pixels detected by the MSI cloud mask. The histograms and scatter plots are shown for ATLID–MSI synergy product (AM-CTH, left) and MSI only product (M-COP, right). The indicator f_i displays the percentage of data points within $\pm i$ m from the 1:1 line.

geometric boundary in case of optically thick clouds such as stratus, nimbostratus and stratocumulus clouds.

425 The number of JSG pixels considered in the histogram is provided in the plots. As previously stated (Section 4.1.2), AM-CTH

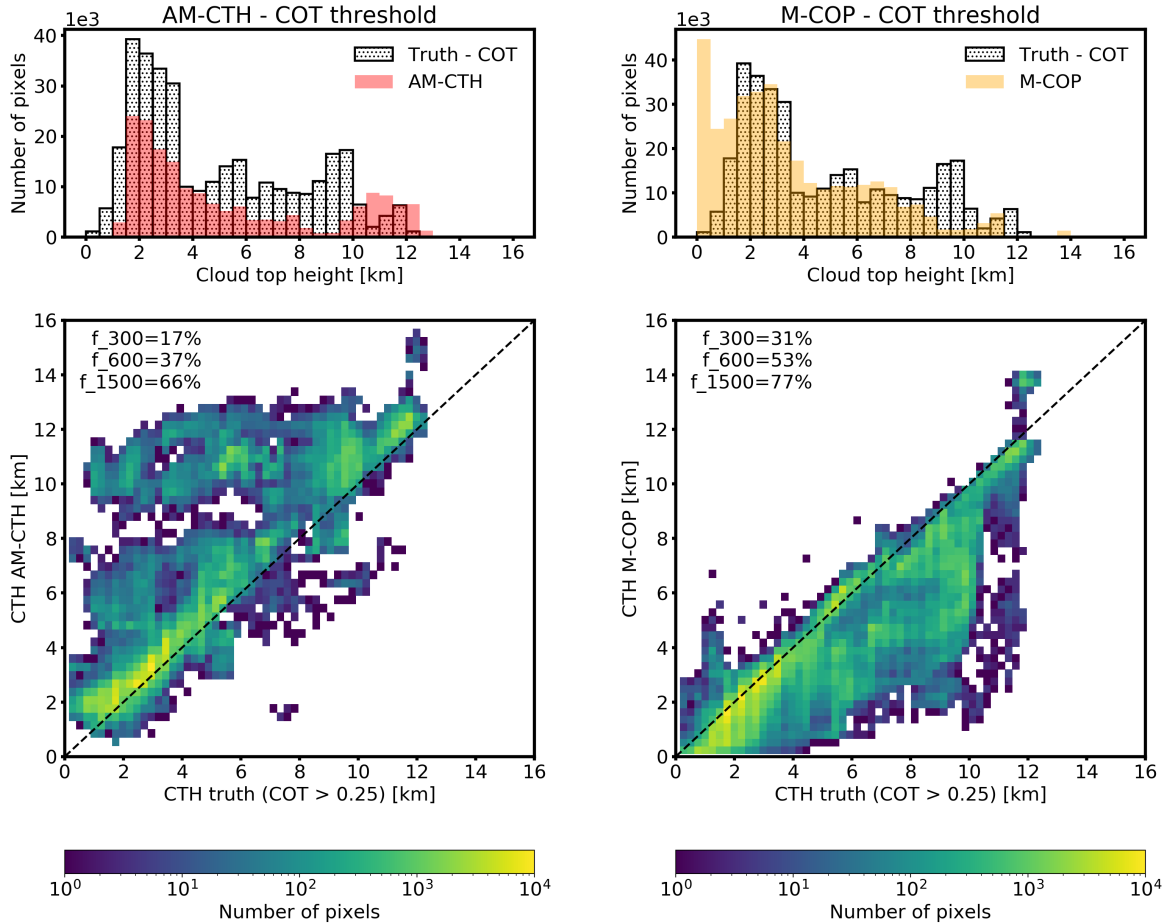


Figure 10. The same as Fig. 9, but here, the true CTH was determined by the MSI-based definition with COT threshold of 0.25.

was able to transfer a CTH difference for half of the CTHs (51%) provided in M-COP in the case of the *Halifax* scene. A special challenge are the multi-layer clouds for which the results are presented in Figure 12. The definition applied to the GEM model output follows the criteria introduced in the A-CTH algorithm (Wandinger et al., 2023b) stating, that at least five height bins corresponding to approximately 500 m of clear air has to be present between two cloud layers to be classified as multi-layer.

430 The multi-layer clouds are not included in the nine ISCCP cloud classes (Fig. 11) but treated on top as a tenth cloud class as

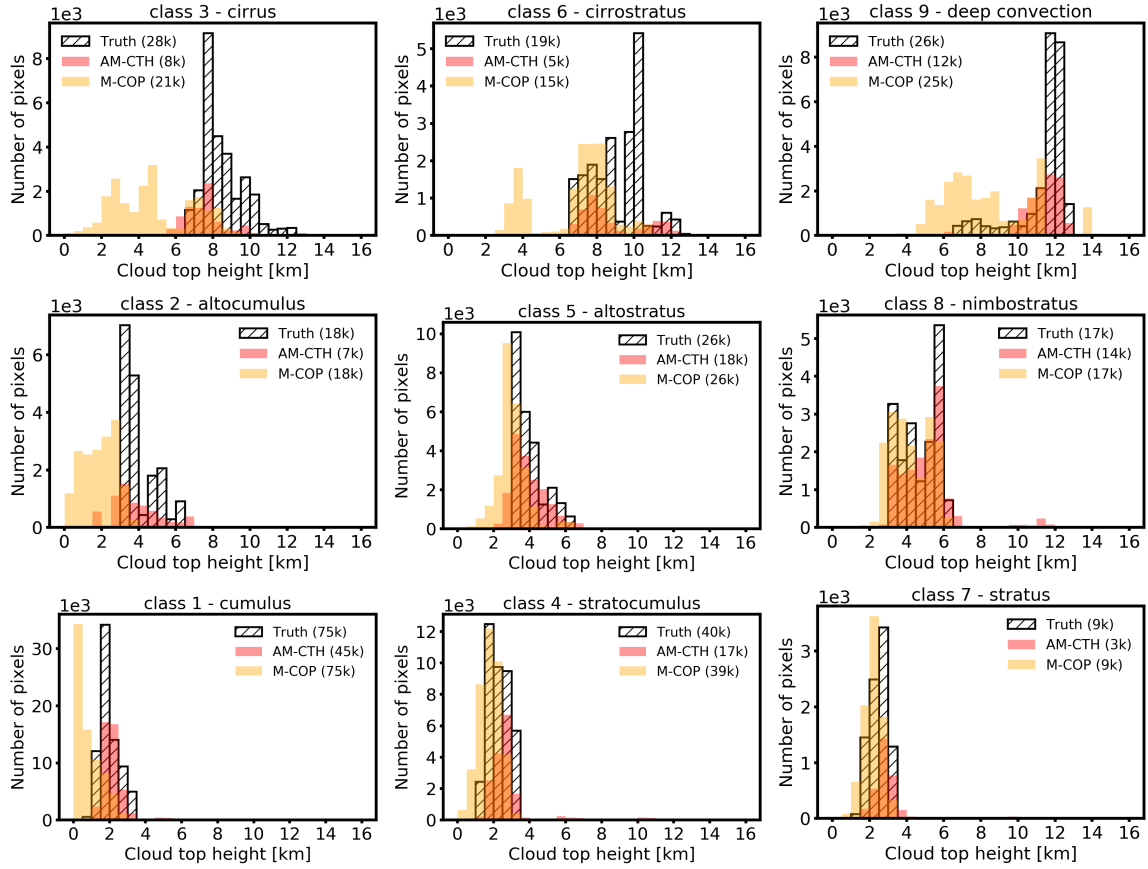


Figure 11. Histograms of the CTH validation against the GEM model truth (hatched) for the nine ISCCP cloud classes. The cloud class was defined by the GEM model truth using an extinction threshold of 20 Mm^{-1} for the CTH detection. The multi-layer clouds are not included. The output of M-COP (orange) and AM-CTH (red) for the same pixel are presented for the *Halifax* scene. In brackets, the total number of pixels in kilo counts is provided for each cloud class.

implemented in the AM-CTH algorithm. The multi-layer clouds are the most frequent cloud class in the *Halifax* scene with 102k JSG pixels. Figure 12 clearly shows that the CTH of the high clouds dominates the multi-layer CTH. Here, AM-CTH significantly improves the (geometric) CTH detection compared to the MSI stand-alone algorithm (M-COP). 41% instead of 2% of the CTHs were detected within $\pm 600 \text{ m}$ from the 1:1 line. The second peak in true CTH between 6 and 8 km height is underestimated by both M-COP and AM-CTH. These clouds are further away from the track and the AM-CTH CTH is based on the MSI measurements. Nevertheless, the ATLID–MSI columnar products improve the CTH detection, especially in the case of multi-layer clouds and single-layer high and optically thin clouds compared to the MSI stand-alone retrieval. MSI is sensitive to the radiative CTH rather than the geometric CTH (see Fig. 8).

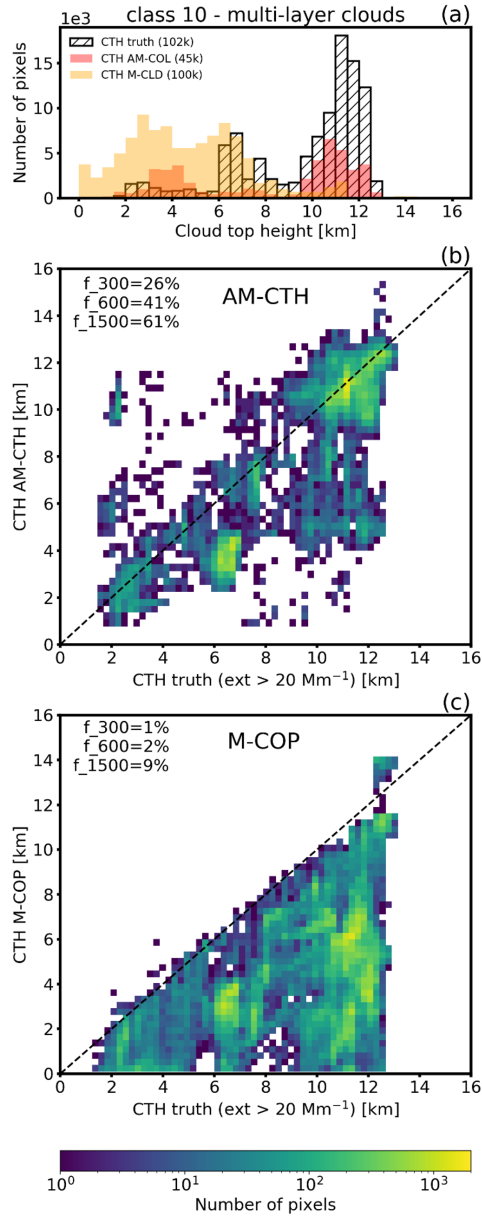


Figure 12. The same as Fig. 11 but for the tenth cloud class "multi-layer" (a). The scatter plots relate the CTH from AM-CTH (b) and M-COP (c) to the model truth based on an extinction threshold of 20 Mm^{-1} . The indicator f_i displays the percentage of data points within $\pm i$ m from the 1:1 line.

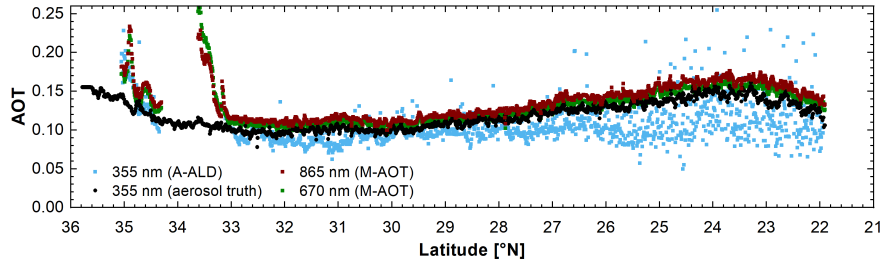


Figure 13. AOT along the ATLID track in the *Halifax aerosol* scene derived by ATLID (355 nm, blue) and MSI (670 nm, green and 865 nm, brown). The true AOT at 355 nm is shown in black **for the aerosol only regardless of the clouds above. The ATLID scene, i.e., the Mie co-polar signal is shown in Fig. 9 of Wandinger et al. (2023b).**

4.2 AM-ACD validation

440 Firstly, the output of the AM-ACD algorithm for the *Halifax aerosol* scene is presented (Sect. 4.2.1). Then, **the more complex aerosol conditions in the *Hawaii* scene are analyzed (Sect. 4.2.2). In the last part, the output of both scenes is validated against the CAMS model truth (Sect. 4.2.3).**

4.2.1 AM-ACD output for the *Halifax aerosol* scene

The *Halifax aerosol* scene is created for the validation of aerosol retrievals and contains solely marine aerosol and some ice clouds. The dominant aerosol type for the cloud-free pixels along track is correctly classified by M-AOT and A-ALD as coarse mode spherical and marine aerosol, respectively. The AOT along track for all wavelengths is shown in Figure 13. M-AOT provides the AOT at 670 nm and 865 nm. A-ALD contains the AOT at 355 nm from the integrated ATLID extinction coefficient. The ice cloud at 34°N is only partly detected by the MSI cloud mask and thus the **optical thickness** of the ice crystals is included in the M-AOT product. At 35°N, the cirrus is even too thin to be detected by A-LAY, which classifies the corresponding profiles as cloud free and starts the aerosol retrievals (A-ALD algorithm). **The additional optical thickness of the ice crystals increases the AOT in the A-ALD product and lead to an overestimation compared to the CAMS model truth AOT which is provided for aerosol only.** The medium resolution output of the extinction coefficient from the A-PRO processor (A-EBD product) is used to calculate the AOT at 355 nm. Especially in the southern part of the scene, the AOT values at 355 nm scatter a lot. The ATLID AOT in this marine-aerosol dominated scene is lower compared to the model truth by -0.0102 ± 0.0659 for the scene $< 32.5^\circ\text{N}$ which is not influenced by the cirrus cloud. Possible reasons for the underestimation of the AOT lie in the extinction calculation of the A-PRO processor (Donovan et al., 2023a). The high standard deviation is caused by the scattering of the ATLID AOT values. Nevertheless, the deviation from the model truth is within the accuracy of 0.05 for the AOT as demanded by the EarthCARE mission requirements (MRD, 2006).

450

455

In the next step, the Ångström exponent (355 nm/670 nm) is calculated along track. The Ångström exponent per dominant aerosol type is obtained by averaging the Ångström exponents for all pixels along track for which the dominant aerosol type

460

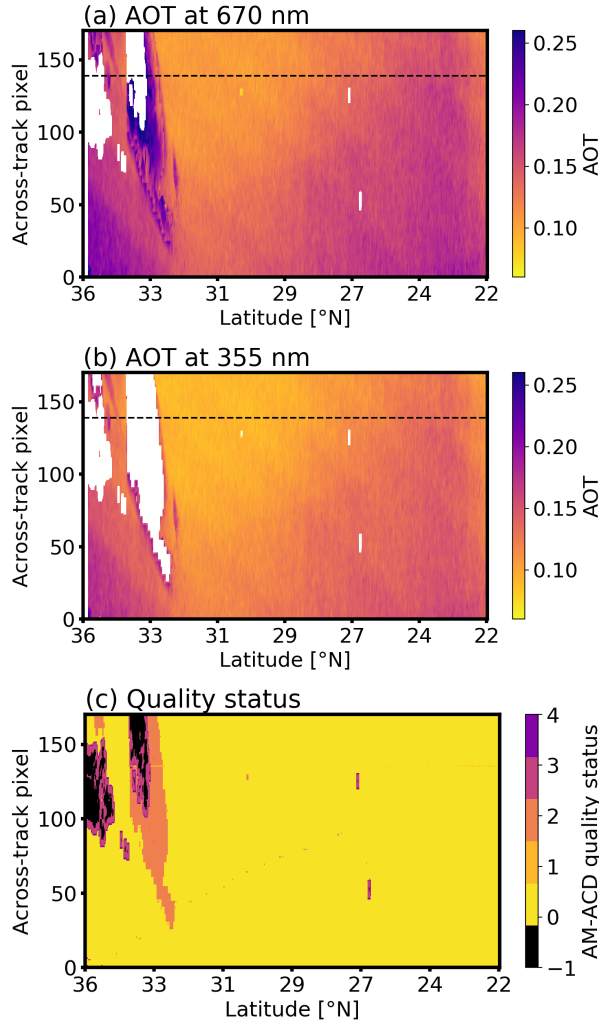


Figure 14. AOT at 670 nm (a) and 355 nm (b) and AM-ACD quality status (c) for the *Halifax aerosol* scene. The ATLID track is marked with a black dashed line, **except for (c) to not overlay the quality status of 1 which is only reported along the track**. For the pixels categorized as cloudy, M-AOT does not derive an AOT (white areas in (a)). Still some ice cloud is present which leads to an increased AOT ($>32.5^{\circ}\text{N}$). The M-AOT algorithm derives a different aerosol mixture for the cloud-influenced pixels. This mixture does not agree along track and therefore these pixels are not considered in the transference of the AOT at 355 nm from the track to the swath (larger white area in (b)). This behavior is reflected in the quality status of AM-ACD (details are provided in the Appendix A2).

of both input algorithms (M-AOT and A-ALD) agrees. Just marine (coarse mode spherical) aerosol is present in the *Halifax aerosol* scene. An Ångström exponent for the other types is not derived as they are not present along track. The derived Ångström exponent for marine aerosol (coarse mode spherical) is -0.28 ± 0.37 . HETEAC defines an Ångström exponent of -0.16 for pure coarse mode spherical aerosol in the respective wavelength range (Wandinger et al., 2023a). The too low ex-

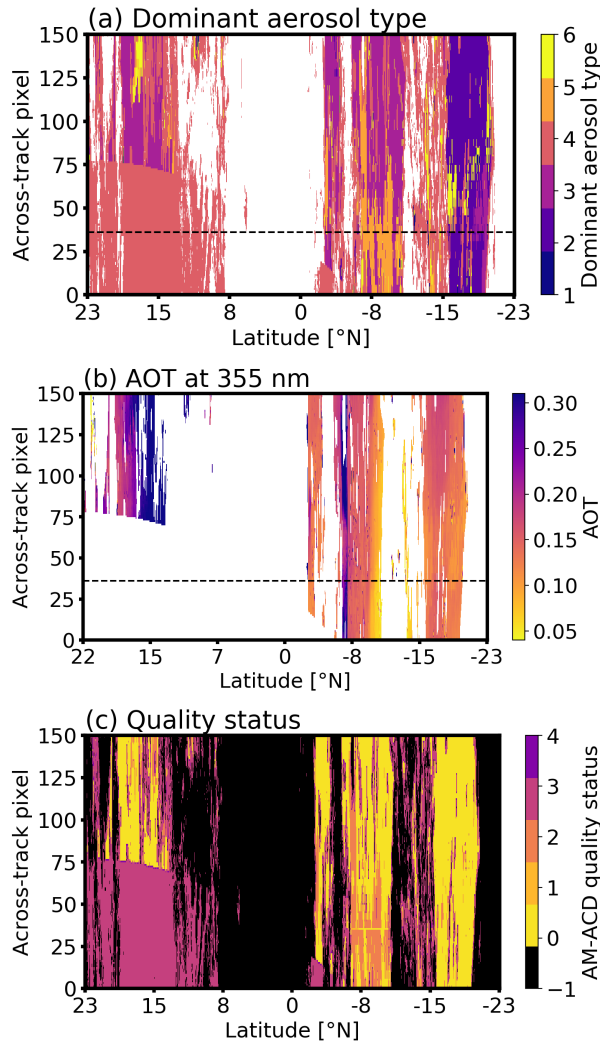


Figure 15. The dominant aerosol type (a), the AOT at 355 nm (b), and AM-ACD quality status (c) for the *Hawaii* scene. The dominant aerosol type numbering follows Table 3: 1 – dust, 2 – marine aerosol, 3 – continental pollution, 4 – smoke, 5 – dusty smoke, 6 – dusty aerosol mix. The ATLID track is marked with a black dashed line, **except for (c) to not overlay the quality status of 1 which is only reported along the track.**

465 tinction coefficient derived from ATLID and the consequently too low AOT at 355 nm is the reason for the deviation of the Ångström exponent. **The scattering in the A-EBD results lead to the high standard deviation.** Nevertheless, the derived Ångström exponent is used to calculate the AOT at 355 nm on the swath from the AOT at 670 nm. The results are presented in Figure 14 together with the quality status of the AM-ACD product.

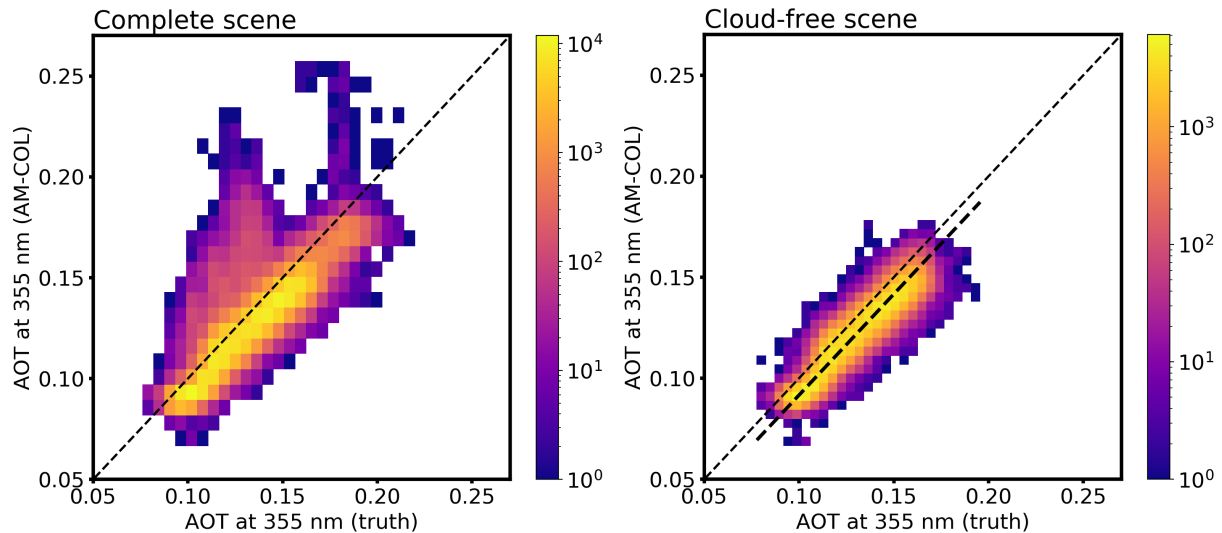


Figure 16. The AOT at 355 nm derived with AM-ACD in the *Halifax aerosol* scene is compared against the model truth. On the left the results for the entire scene are shown. The cirrus clouds lead to an overestimation of the AOT. On the right, the scene is shown for a latitude $<32.5^\circ\text{N}$, there no cloud is present (see Fig. 14). Under cloud-free conditions, the AOT is underestimated. The linear fit shown as thick dashed line indicates the mean offset of -0.0083 ± 0.0066 .

470 4.2.2 AM-ACD output for the *Hawaii* scene

More aerosol types are present in the *Hawaii* scene which will be shown to demonstrate the performance under complex aerosol situations. The dominant aerosol type shown in Figure 15a was derived from the M-AOT aerosol mixing ratios as described in Section 3.2.1. Most of the scene is dominated by fine mode aerosol which is classified as smoke, continental pollution and dusty smoke because of similar optical properties. Only south of 16°S , marine aerosol dominates. A wide
 475 area on the northern Hemisphere is affected by sun glint which leads to an increased uncertainty in the M-AOT product. In these areas, the quality status of AM-ACD is 3 as seen in Figure 15c. Thus, in the following we focus on the Southern hemispheric part of the *Hawaii* scene. The obtained AOT at 355 nm is presented in Figure 15b. The comparison with the model truth is provided in the next subsection.

4.2.3 Aerosol product validation against the model truth

480 The AM-ACD products are validated against the model truth available for the simulated test scenes. **Firstly, we discuss the *Halifax aerosol* scene and then the *Hawaii* scene.**

In the *Halifax aerosol* scene, the dominant aerosol type agrees for the entire scene (not shown). The AOT at 670 and 865 nm are taken from the M-AOT product (now provided on JSG) and are validated in Docter et al. (2023). The validation of the AOT at 355 nm on the MSI swath is presented in Figure 16. The high AOT values between 0.20 and 0.25 which are not present in

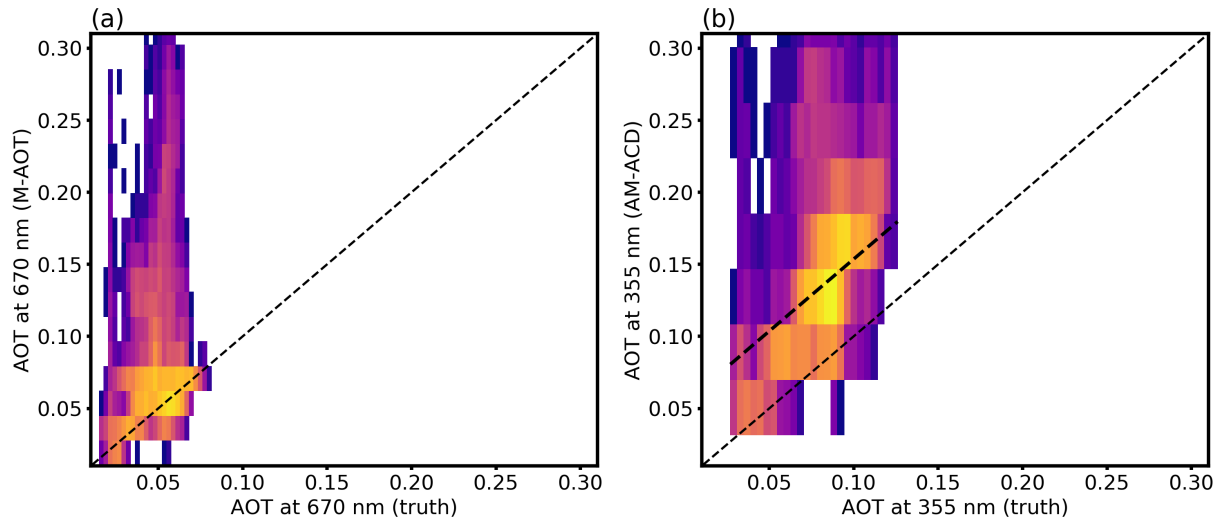


Figure 17. The AOT at 670 nm from M-AOT and at 355 nm from AM-ACD in the *Hawaii* scene is compared against the model truth. Here, the results are shown for the southern hemisphere and just for the pixel with an AM-ACD quality status of 0. The thick dashed line indicates the mean offset of 0.054 found for the AOT at 355 nm.

the model truth are caused by an incorrect aerosol-cloud discrimination. The validation is done for latitudes $< 32.5^{\circ}\text{N}$ which are not influenced by any cloud (right part in Fig. 16). The majority of the pixels follows the 1:1 line with a small negative offset of -0.0083 ± 0.0066 . The offset is caused by the negative offset of the AOT at 355 nm from upstream processors namely the extinction calculations in A-PRO (-0.0102 ± 0.0659).

In the case of the *Hawaii* scene, the agreement is less good. In Figure 17, we compare first the AOT at 670 nm against the model truth and see that the majority of the pixels follow the 1:1 line. The comparison is restricted to the southern hemisphere and an AM-ACD quality status of 0. The overestimation of the AOT at 670 nm by the M-AOT algorithm is caused by thin cirrus clouds which are not detected by M-CM. Therefore, these pixels are processed by the aerosol algorithm and lead to an increased AOT. AM-ACD uses the AOT at 670 nm to calculate the AOT at 355 nm on the swath. Therefore, this overestimation continues in the AM-ACD product. Moreover, the overestimation increases for the AOT at 355 nm. A mean offset of 0.054 (indicated by the dashed line) was found under these complex aerosol conditions. It is slightly above the mission requirements of 0.05. The main reason for the overestimation can be attributed to the presence of thin cirrus clouds which could not be detected by the MSI cloud mask.

In summary, the method applied in the AM-ACD algorithm itself leads to a good agreement with the model truth in the case of the simple *Halifax aerosol* scene. Even for the more complex aerosol situation in the *Hawaii* scene, the results are only slightly above the mission requirements. The AOT validation at 355 or 670 nm across all simulated test scenes for various processors (e.g., A-EBD, M-AOT and ACM-CAP) is provided in chapter 3.4 of Mason et al. (2023a).

5 Conclusions

The synergistic ATLID–MSI Column Products (AM-COL) processor combines the strengths of ATLID in vertically-resolved profiles of aerosol and clouds with the benefits of MSI in observing the complete scene besides the track of the satellite. The uncertainties in the MSI CTH detection and MSI aerosol typing were the driving motivation to develop this synergistic L2b algorithm. The two instruments are compared along the satellite track where they observe the same atmospheric scene. The main task of the AM-COL algorithm is to transfer this combined information from the track to the MSI swath (swath width 150 km). The algorithm is split into the analysis of cloudy pixels (AM-CTH product) and cloud-free pixels for aerosol observations (AM-ACD product) based on the MSI cloud mask.

The AM-CTH algorithm produces the synergistic CTH difference measured along the track and transfers this difference to the swath. Several similarity criteria are used to relate an across-track pixel to an along-track pixel: agreement in cloud type, cloud phase, surface type, **satisfaction of** a brightness temperature difference (at 10.8 μm) and a reflectance difference (at 0.67 μm) threshold. For the simulated EarthCARE test scenes, it could be shown that the vertical information of ATLID improves the detection of cirrus CTHs compared to the MSI stand-alone retrieval. In addition, the CTH of cumulus and altocumulus clouds improves if ATLID input is used. The MSI retrieval underestimates the CTH of these cloud types. The usage of the simulated test scenes allows us to study the different definitions of the CTH by using an extinction threshold or a COT threshold. The first one describes the geometric boundary of the cloud as it is seen by the lidar and the latter one describes the radiative CTH as it is seen by the imager. Special care has to be taken in case of multi-layer cloud scenarios. The improved cirrus detection of the ATLID–MSI synergy improved the multi-layer CTH determination in the simulated test scenes. However, the brightness temperature difference between 10.8 and 12.0 μm was not sensitively enough simulated to clearly detect multi-layer cloud scenarios by MSI. Here, adaptations will become necessary once real EarthCARE data are available. The synergistic approach of a lidar and an imager on the same platform will provide insight into multi-layer cloud scenarios and their influence on passive sensors.

The AM-ACD algorithm combines the AOT observations at 355 nm from ATLID and at 670 and 865 nm from MSI to deliver an Ångström exponent. ATLID is a single-wavelength lidar and MSI has a limited amount of wavelengths at its disposal. Therefore, the Ångström exponent adds valuable input to the aerosol classification. Along track a comparison of the dominant aerosol type from MSI retrieval and the columnar aerosol classification from ATLID is possible. In case of agreement, the Ångström exponent (355 nm/670 nm) is derived. It is used to transfer the AOT at 355 nm to the swath where the MSI observations at 670 nm are available. In this way, aerosol plumes are tracked from the track to the swath. The aerosol vertical distribution has an impact on the passive AOD retrieval as shown by Wu et al. (2017). EarthCARE is ideally designed to further studying this effect and to develop proper corrections based on ATLID’s vertical information.

The paper describes the current stage of the AM-CTH and AM-ACD algorithms. Improvements and adaptations will become necessary once real EarthCARE data are available. Suborbital observations on the track and swath are necessary to further validate the AM-CTH and AM-ACD products during the validation phase of EarthCARE. The columnar products are designed to improve the MSI retrievals by adding the vertical and spectral information from ATLID. The combination of active and

passive remote-sensing observations with close colocation will create a valuable dataset and enhance our experience for future passive satellite missions.

Data availability. The simulated test data sets and the AM-COL processor outputs are available at <https://zenodo.org/record/7311704> (van
540 Zadelhoff et al., 2022).

Author contributions. UW, AH and MH designed and implemented the algorithm. MH validated it against the model truth. ND, DD and GvZ provided valuable comments on the algorithm throughout many years. SB supported the validation against the GEM model truth. MH wrote the manuscript in strong collaboration with the coauthors.

Competing interests. UW is member of the editorial board of Atmospheric Measurement Techniques and co-editor of the Special Issue to
545 which this paper contributes. The peer-review process was guided by an independent editor. The authors declare that they have no conflict of interest.

Acknowledgements. This work has been funded by ESA grants 4000112018/14/NL/CT (APRIL) and 4000134661/21/NL/AD (CARDI-
NAL). We thank Tobias Wehr (deceased) and Michael Eisinger for their continuous support over many years and the EarthCARE developer
550 teams for valuable discussions in various meetings. We are grateful to Florian Schneider and Stefan Horn for the basic implementation of the code in Fortran and to Athena Floutsi for her support in describing the aerosol types in terms of HETEAC aerosol components. We thank Eleni Marinou and an anonymous reviewer for their careful reading and their expert comments to our manuscript.

Appendix A: Quality status

A1 Quality status of the AM-CTH product

The quality status of the cloud top height product (Q_{CTH}) is provided for each JSG pixel along and across track on a scale from 0 (highest quality) to 4 (bad quality). A quality status of -1 is used for JSG pixels for which no cloud was detected by M-CM.

The steps of the quality status are the following:

- $Q_{CTH} = 0$: Good data, high quality. Agreement of the across-track pixel was found within ± 2 pixel along track.
- $Q_{CTH} = 1$: Valid data, but agreement was found in a configurable search distance (default 75) North or South of the corresponding pixel along track.
- $Q_{CTH} = 2$: Warning: A-LAY detected multi-layer cloud scenario for the along-track pixel which was used to transfer the CTH difference to the swath.
- $Q_{CTH} = 3$: Warning: Degraded quality due to twilight or night conditions.
- $Q_{CTH} = 4$: Bad data. Observations on MSI grid are not consistent on JSG.
- $Q_{CTH} = -1$: Not surely cloudy according to M-CM.

A2 Quality status of the AM-ACD product

The quality status of the aerosol columnar descriptor (Q_{ACD}) is provided for each JSG pixel along and across track on a scale from 0 (highest quality) to 4 (bad quality). A quality status of -1 is used for JSG pixels for which a cloud was detected by M-CM. The quality status is determined along track where ATLID and MSI information is available. Using the homogeneity criteria provided by M-AOT the quality status is transferred to the MSI swath. The steps of the quality status are the following:

- $Q_{ACD} = 0$: **Good data, high quality of M-AOT input.**
- $Q_{ACD} = 1$: **Warning: A significant amount of ice ($> 20\%$ (configurable) in terms of AOT) was detected by A-TC (provided in A-ALD). This warning is provided along track only, but probably holds for the close swath pixel as well.**
- $Q_{ACD} = 2$: **Warning: Dominant aerosol type on swath was not present along the track, AOT at 355 nm could not be calculated.**
- $Q_{ACD} = 3$: **Warning: The homogeneity criteria of M-AOT are not fulfilled.**
- $Q_{ACD} = 4$: **Bad data. Observations on MSI grid are not consistent on JSG.**
- $Q_{ACD} = -1$: Not surely cloud free according to M-CM.

References

- 565 Ansmann, A., Wandinger, U., Rille, O. L., Lajas, D., and Straume, A. G.: Particle backscatter and extinction profiling with the spaceborne high-spectral-resolution Doppler lidar ALADIN: methodology and simulations, *Appl. Opt.*, 46, 6606–6622, <https://doi.org/10.1364/AO.46.006606>, 2007.
- Barker, H. W., Cole, J. N. S., Qu, Z., Villefranche, N., and Shephard, M.: Radiative closure assessment of retrieved cloud and aerosol properties for the EarthCARE mission: the ACMB-DF product, *Atmospheric Measurement Techniques*, to be submitted, 2023.
- 570 Baum, B. A., Menzel, W. P., Frey, R. A., Tobin, D. C., Holz, R. E., Ackerman, S. A., Heidinger, A. K., and Yang, P.: MODIS Cloud-Top Property Refinements for Collection 6, *Journal of Applied Meteorology and Climatology*, 51, 1145 – 1163, <https://doi.org/10.1175/JAMC-D-11-0203.1>, 2012.
- Burton, S. P., Ferrare, R. A., Hostetler, C. A., Hair, J. W., Rogers, R. R., Obland, M. D., Butler, C. F., Cook, A. L., Harper, D. B., and Froyd, K. D.: Aerosol classification using airborne High Spectral Resolution Lidar measurements – methodology and examples, *Atmospheric*
- 575 *Measurement Techniques*, 5, 73–98, <https://doi.org/10.5194/amt-5-73-2012>, 2012.
- Chan, M. A. and Comiso, J. C.: Cloud features detected by MODIS but not by CloudSat and CALIOP, *Geophysical Research Letters*, 38, <https://doi.org/https://doi.org/10.1029/2011GL050063>, 2011.
- Compernelle, S., Argyrouli, A., Lutz, R., Sneep, M., Lambert, J.-C., Fjæraa, A. M., Hubert, D., Keppens, A., Loyola, D., O’Connor, E., Romahn, F., Stammes, P., Verhoelst, T., and Wang, P.: Validation of the Sentinel-5 Precursor TROPOMI cloud data with Cloudnet, Aura
- 580 OMI O₂–O₂, MODIS, and Suomi-NPP VIIRS, *Atmospheric Measurement Techniques*, 14, 2451–2476, <https://doi.org/10.5194/amt-14-2451-2021>, 2021.
- de Leeuw, G., Holzer-Popp, T., Bevan, S., Davies, W. H., Descloîtres, J., Grainger, R. G., Griesfeller, J., Heckel, A., Kinne, S., Klüser, L., Kolmonen, P., Litvinov, P., Martynenko, D., North, P., Ovigneur, B., Pascal, N., Poulsen, C., Ramon, D., Schulz, M., Siddans, R., Sogacheva, L., Tanré, D., Thomas, G. E., Virtanen, T. H., von Hoyningen Huene, W., Vountas, M., and Pinnock, S.: Evaluation
- 585 of seven European aerosol optical depth retrieval algorithms for climate analysis, *Remote Sensing of Environment*, 162, 295–315, <https://doi.org/https://doi.org/10.1016/j.rse.2013.04.023>, 2015.
- do Carmo, J., de Villele, G., Wallace, K., Lefebvre, A., Ghose, K., Kanitz, T., Chassat, F., Corselle, B., Belhadj, T., and Bravetti, P.: ATmo-spheric LIDar (ATLID): Pre-Launch Testing and Calibration of the European Space Agency Instrument That Will Measure Aerosols and Thin Clouds in the Atmosphere, *Atmosphere*, 12, 76, 2021.
- 590 Docter, N., Preusker, R., Filipitsch, F., Kritten, L., Schmidt, F., and Fischer, J.: Aerosol optical depth retrieval from the EarthCARE Multi-Spectral Imager: the M-AOT product, *Atmospheric Measurement Techniques*, 16, 3437–3457, <https://doi.org/10.5194/amt-16-3437-2023>, 2023.
- Donovan, D., van Zadelhoff, G.-J., and Wang, P.: The ATLID L2a profile processor (A-AER, A-EBD, A-TC and A-ICE products), *Atmo-spheric Measurement Techniques*, to be submitted, 2023a.
- 595 Donovan, D. P., Kollias, P., Velázquez Blázquez, A., and van Zadelhoff, G.-J.: The Generation of EarthCARE L1 Test Data sets Using Atmospheric Model Data Sets, *EGUsphere*, 2023, 1–54, <https://doi.org/10.5194/egusphere-2023-384>, 2023b.
- Eisinger, M., Wehr, T., Kubota, T., Bernaerts, D., and Wallace, K.: The EarthCARE Mission - Science Data Processing Chain Overview, *Atmospheric Measurement Techniques*, to be submitted, 2023.

- Flament, T., Trapon, D., Lacour, A., Dabas, A., Ehlers, F., and Huber, D.: Aeolus L2A aerosol optical properties product: standard correct
600 algorithm and Mie correct algorithm, *Atmospheric Measurement Techniques*, 14, 7851–7871, <https://doi.org/10.5194/amt-14-7851-2021>, 2021.
- Floutsi, A. A., Baars, H., Engelmann, R., Althausen, D., Ansmann, A., Bohlmann, S., Heese, B., Hofer, J., Kanitz, T., Haarig, M., Ohneiser, K., Radenz, M., Seifert, P., Skupin, A., Yin, Z., Abdullaev, S. F., Komppula, M., Filioglou, M., Giannakaki, E., Stachlewska, I. S., Janicka, L., Bortoli, D., Marinou, E., Amiridis, V., Gialitaki, A., Mamouri, R.-E., Barja, B., and Wandinger, U.: DeLiAn – a growing collection
605 of depolarization ratio, lidar ratio and Ångström exponent for different aerosol types and mixtures from ground-based lidar observations, *Atmospheric Measurement Techniques*, 16, 2353–2379, <https://doi.org/10.5194/amt-16-2353-2023>, 2023.
- Fritz, S. and Winston, J. S.: SYNOPTIC USE OF RADIATION MEASUREMENTS FROM SATELLITE TIROS II, *Monthly Weather Review*, 90, 1 – 9, [https://doi.org/10.1175/1520-0493\(1962\)090<0001:SUORMF>2.0.CO;2](https://doi.org/10.1175/1520-0493(1962)090<0001:SUORMF>2.0.CO;2), 1962.
- Griesche, H. J., Seifert, P., Ansmann, A., Baars, H., Barrientos Velasco, C., Bühl, J., Engelmann, R., Radenz, M., Zhenping, Y., and Macke, A.: Application of the shipborne remote sensing supersite OCEANET for profiling of Arctic aerosols and clouds during *Polarstern* cruise PS106, *Atmospheric Measurement Techniques*, 13, 5335–5358, <https://doi.org/10.5194/amt-13-5335-2020>, 2020.
610
- Groß, S., Freudenthaler, V., Wirth, M., and Weinzierl, B.: Towards an aerosol classification scheme for future EarthCARE lidar observations and implications for research needs, *Atmospheric Science Letters*, 16, 77–82, <https://doi.org/10.1002/asl2.524>, 2015.
- Håkansson, N., Adok, C., Thoss, A., Scheirer, R., and Hörnquist, S.: Neural network cloud top pressure and height for MODIS, *Atmospheric Measurement Techniques*, 11, 3177–3196, <https://doi.org/10.5194/amt-11-3177-2018>, 2018.
615
- Holz, R. E., Ackerman, S. A., Nagle, F. W., Frey, R., Dutcher, S., Kuehn, R. E., Vaughan, M. A., and Baum, B.: Global Moderate Resolution Imaging Spectroradiometer (MODIS) cloud detection and height evaluation using CALIOP, *Journal of Geophysical Research: Atmospheres*, 113, <https://doi.org/https://doi.org/10.1029/2008JD009837>, 2008.
- Holzer-Popp, T., de Leeuw, G., Griesfeller, J., Martynenko, D., Klüser, L., Bevan, S., Davies, W., Ducos, F., Deuzé, J. L., Graigner, R. G., Heckel, A., von Hoyningen-Hüne, W., Kolmonen, P., Litvinov, P., North, P., Poulsen, C. A., Ramon, D., Siddans, R., Sogacheva, L., Tanre, D., Thomas, G. E., Vountas, M., Descloîtres, J., Griesfeller, J., Kinne, S., Schulz, M., and Pinnock, S.: Aerosol retrieval experiments in the ESA Aerosol_cci project, *Atmospheric Measurement Techniques*, 6, 1919–1957, <https://doi.org/10.5194/amt-6-1919-2013>, 2013.
620
- Hünerbein, A., Bley, S., Deneke, H., Meirink, J. F., van Zadelhoff, G.-J., and Walther, A.: Cloud optical and physical properties retrieval from EarthCARE multi-spectral imager: the M-COP products, *EGUsphere*, 2023, 1–23, <https://doi.org/10.5194/egusphere-2023-305>, 2023a.
- Hünerbein, A., Bley, S., Horn, S., Deneke, H., and Walther, A.: Cloud mask algorithm from the EarthCARE Multi-Spectral Imager: the M-CM products, *Atmospheric Measurement Techniques*, 16, 2821–2836, <https://doi.org/10.5194/amt-16-2821-2023>, 2023b.
625
- Illingworth, A. J., Barker, H. W., Beljaars, A., Ceccaldi, M., Chepfer, H., Clerbaux, N., Cole, J., Delanoë, J., Domenech, C., Donovan, D. P., Fukuda, S., Hiraoka, M., Hogan, R. J., Huenerbein, A., Kollias, P., Kubota, T., Nakajima, T., Nakajima, T. Y., Nishizawa, T., Ohno, Y., Okamoto, H., Oki, R., Sato, K., Satoh, M., Shephard, M. W., Velázquez-Belázquez, A., Wandinger, U., Wehr, T., and van Zadelhoff, G.-J.: The EarthCARE Satellite: The Next Step Forward in Global Measurements of Clouds, Aerosols, Precipitation, and Radiation, *Bulletin of the American Meteorological Society*, 96, 1311–1332, <https://doi.org/10.1175/BAMS-D-12-00227.1>, 2015.
630
- Irbah, A., Delanoë, J., van Zadelhoff, G.-J., Donovan, D. P., Kollias, P., Puigdomènech Treserras, B., Mason, S., Hogan, R. J., and Tatarevic, A.: The classification of atmospheric hydrometeors and aerosols from the EarthCARE radar and lidar: the A-TC, C-TC and AC-TC products, *Atmospheric Measurement Techniques*, 16, 2795–2820, <https://doi.org/10.5194/amt-16-2795-2023>, 2023.
- Iwabuchi, H., Saito, M., Tokoro, Y., Putri, N. S., and Sekiguchi, M.: Retrieval of radiative and microphysical properties of clouds from multispectral infrared measurements, *Progress in Earth and Planetary Science*, 3, 32, <https://doi.org/10.1186/s40645-016-0108-3>, 2016.
635

- Kim, M.-H., Omar, A. H., Tackett, J. L., Vaughan, M. A., Winker, D. M., Trepte, C. R., Hu, Y., Liu, Z., Poole, L. R., Pitts, M. C., Kar, J., and Magill, B. E.: The CALIPSO version 4 automated aerosol classification and lidar ratio selection algorithm, *Atmospheric Measurement Techniques*, 11, 6107–6135, <https://doi.org/10.5194/amt-11-6107-2018>, 2018.
- 640 Kinne, S., O'Donnel, D., Stier, P., Kloster, S., Zhang, K., Schmidt, H., Rast, S., Giorgetta, M., Eck, T. F., and Stevens, B.: MAC-v1: A new global aerosol climatology for climate studies, *Journal of Advances in Modeling Earth Systems*, 5, 704–740, <https://doi.org/https://doi.org/10.1002/jame.20035>, 2013.
- Kollias, P., Puidgomènech Treserras, B., Battaglia, A., Borque, P. C., and Tatarevic, A.: Processing reflectivity and Doppler velocity from EarthCARE's cloud-profiling radar: the C-FMR, C-CD and C-APC products, *Atmospheric Measurement Techniques*, 16, 1901–1914, 645 <https://doi.org/10.5194/amt-16-1901-2023>, 2023.
- Loyola, D. G., Gimeno García, S., Lutz, R., Argyrouli, A., Romahn, F., Spurr, R. J. D., Pedergrana, M., Doicu, A., Molina García, V., and Schüssler, O.: The operational cloud retrieval algorithms from TROPOMI on board Sentinel-5 Precursor, *Atmospheric Measurement Techniques*, 11, 409–427, <https://doi.org/10.5194/amt-11-409-2018>, 2018.
- Mahesh, A., Gray, M. A., Palm, S. P., Hart, W. D., and Spinhirne, J. D.: Passive and active detection of clouds: Comparisons between MODIS 650 and GLAS observations, *Geophysical Research Letters*, 31, <https://doi.org/https://doi.org/10.1029/2003GL018859>, 2004.
- Mason, S. L., Cole, J. N. S., Docter, N., Donovan, D. P., Hogan, R. J., Hünerbein, A., Kollias, P., Puigdomènech Treserras, B., Qu, Z., Wandinger, U., and van Zadelhoff, G.-J.: An intercomparison of EarthCARE cloud, aerosol and precipitation retrieval products, *EGU-sphere*, 2023, 1–34, <https://doi.org/10.5194/egusphere-2023-1682>, 2023a.
- Mason, S. L., Hogan, R. J., Bozzo, A., and Pounder, N. L.: A unified synergistic retrieval of clouds, aerosols, and precipitation from 655 EarthCARE: the ACM-CAP product, *Atmospheric Measurement Techniques*, 16, 3459–3486, <https://doi.org/10.5194/amt-16-3459-2023>, 2023b.
- Min, M., Li, J., Wang, F., Liu, Z., and Menzel, W. P.: Retrieval of cloud top properties from advanced geostationary satellite imager measurements based on machine learning algorithms, *Remote Sensing of Environment*, 239, 111616, <https://doi.org/https://doi.org/10.1016/j.rse.2019.111616>, 2020.
- 660 Minnis, P., Yost, C. R., Sun-Mack, S., and Chen, Y.: Estimating the top altitude of optically thick ice clouds from thermal infrared satellite observations using CALIPSO data, *Geophysical Research Letters*, 35, <https://doi.org/https://doi.org/10.1029/2008GL033947>, 2008.
- Mitra, A., Di Girolamo, L., Hong, Y., Zhan, Y., and Mueller, K. J.: Assessment and Error Analysis of Terra-MODIS and MISR Cloud-Top Heights Through Comparison With ISS-CATS Lidar, *Journal of Geophysical Research: Atmospheres*, 126, e2020JD034281, <https://doi.org/https://doi.org/10.1029/2020JD034281>, e2020JD034281 2020JD034281, 2021.
- 665 MRD: EarthCARE Mission Requirements Document, Earth and Mission Science Division, European Space Agency, <https://doi.org/10.5270/esa.earthcare-mrd.2006>, 2006.
- Naud, C., Muller, J.-P., and de Valk, P.: On the use of ICESAT-GLAS measurements for MODIS and SEVIRI cloud-top height accuracy assessment, *Geophysical Research Letters*, 32, <https://doi.org/https://doi.org/10.1029/2005GL023275>, 2005.
- Omar, A. H., Winker, D. M., Vaughan, M. A., Hu, Y., Trepte, C. R., Ferrare, R. A., Lee, K.-P., Hostetler, C. A., Kittaka, C., Rogers, R. R., 670 Kuehn, R. E., and Liu, Z.: The CALIPSO Automated Aerosol Classification and Lidar Ratio Selection Algorithm, *Journal of Atmospheric and Oceanic Technology*, 26, 1994–2014, <https://doi.org/10.1175/2009JTECHA1231.1>, 2009.
- Pavolonis, M. J. and Heidinger, A. K.: Daytime Cloud Overlap Detection from AVHRR and VIIRS, *Journal of Applied Meteorology*, 43, 762 – 778, <https://doi.org/10.1175/2099.1>, 2004.

- Penning de Vries, M. J. M., Beirle, S., Hörmann, C., Kaiser, J. W., Stammes, P., Tilstra, L. G., Tuinder, O. N. E., and Wagner, T.: A global aerosol classification algorithm incorporating multiple satellite data sets of aerosol and trace gas abundances, *Atmospheric Chemistry and Physics*, 15, 10597–10618, <https://doi.org/10.5194/acp-15-10597-2015>, 2015.
- Qu, Z., Donovan, D. P., Barker, H. W., Cole, J. N. S., Shephard, M. W., and Huijnen, V.: Numerical Model Generation of Test Frames for Pre-launch Studies of EarthCARE's Retrieval Algorithms and Data Management System, *Atmospheric Measurement Techniques Discussions*, 2022, 1–31, <https://doi.org/10.5194/amt-2022-300>, 2022.
- Qu, Z., Barker, H. W., Cole, J. N. S., and Shephard, M. W.: Across-track extension of retrieved cloud and aerosol properties for the EarthCARE mission: the ACMB-3D product, *Atmospheric Measurement Techniques*, 16, 2319–2331, <https://doi.org/10.5194/amt-16-2319-2023>, 2023.
- Robbins, D., Poulsen, C., Siems, S., and Proud, S.: Improving discrimination between clouds and optically thick aerosol plumes in geostationary satellite data, *Atmospheric Measurement Techniques*, 15, 3031–3051, <https://doi.org/10.5194/amt-15-3031-2022>, 2022.
- Rossow, W. B. and Schiffer, R. A.: Advances in Understanding Clouds from ISCCP, *Bulletin of the American Meteorological Society*, 80, 2261 – 2288, [https://doi.org/10.1175/1520-0477\(1999\)080<2261:AIUCFI>2.0.CO;2](https://doi.org/10.1175/1520-0477(1999)080<2261:AIUCFI>2.0.CO;2), 1999.
- Russell, P. B., Kacenelenbogen, M., Livingston, J. M., Hasekamp, O. P., Burton, S. P., Schuster, G. L., Johnson, M. S., Knobelspiesse, K. D., Redemann, J., Ramachandran, S., and Holben, B.: A multiparameter aerosol classification method and its application to retrievals from spaceborne polarimetry, *Journal of Geophysical Research: Atmospheres*, 119, 9838–9863, <https://doi.org/https://doi.org/10.1002/2013JD021411>, 2014.
- Sayer, A. M., Lelli, L., Cairns, B., van Diedenhoven, B., Ibrahim, A., Knobelspiesse, K. D., Korkin, S., and Werdell, P. J.: The CHROMA cloud-top pressure retrieval algorithm for the Plankton, Aerosol, Cloud, ocean Ecosystem (PACE) satellite mission, *Atmospheric Measurement Techniques*, 16, 969–996, <https://doi.org/10.5194/amt-16-969-2023>, 2023.
- Smith, W. L. and Platt, C. M. R.: Comparison of Satellite-Deduced Cloud Heights with Indications from Radiosonde and Ground-Based Laser Measurements, *Journal of Applied Meteorology and Climatology*, 17, 1796 – 1802, [https://doi.org/10.1175/1520-0450\(1978\)017<1796:COSDCH>2.0.CO;2](https://doi.org/10.1175/1520-0450(1978)017<1796:COSDCH>2.0.CO;2), 1978.
- Stengel, M., Mieruch, S., Jerg, M., Karlsson, K.-G., Scheirer, R., Maddux, B., Meirink, J., Poulsen, C., Siddans, R., Walther, A., and Hollmann, R.: The Clouds Climate Change Initiative: Assessment of state-of-the-art cloud property retrieval schemes applied to AVHRR heritage measurements, *Remote Sensing of Environment*, 162, 363–379, <https://doi.org/https://doi.org/10.1016/j.rse.2013.10.035>, 2015.
- Stoffelen, A., Paillex, J., Källén, E., Vaughan, J. M., Isaksen, I., Flamant, P., Wergen, W., Andersson, E., Schyberg, H., Culoma, A., Meynart, R., Endemann, M., and Ingmann, P.: THE ATMOSPHERIC DYNAMICS MISSION FOR GLOBAL WIND FIELD MEASUREMENT, *Bulletin of the American Meteorological Society*, 86, 73 – 88, <https://doi.org/10.1175/BAMS-86-1-73>, 2005.
- Tan, Z., Ma, S., Liu, C., Teng, S., Xu, N., Hu, X., Zhang, P., and Yan, W.: Assessing Overlapping Cloud Top Heights: An Extrapolation Method and Its Performance, *IEEE Transactions on Geoscience and Remote Sensing*, 60, 1–11, <https://doi.org/10.1109/TGRS.2022.3170054>, 2022.
- Toledano, C., Cachorro, V. E., Berjon, A., de Frutos, A. M., Sorribas, M., de la Morena, B. A., and Goloub, P.: Aerosol optical depth and Ångström exponent climatology at El Arenosillo AERONET site (Huelva, Spain), *Quarterly Journal of the Royal Meteorological Society*, 133, 795–807, <https://doi.org/10.1002/qj.54>, 2007.
- van Zadelhoff, G.-J., Barker, H. W., Baudrez, E., Bley, S., Clerbaux, N., Cole, J. N. S., de Kloe, J., Docter, N., Domenech, C., Donovan, D. P., Dufresne, J.-L., Eisinger, M., Fischer, J., García-Marañón, R., Haarig, M., Hogan, R. J., Hünerbein, A., Kollias, P., Koopman, R., Madenach, N., Mason, S. L., Preusker, R., Puigdomènech Treserras, B., Qu, Z., Ruiz-Saldaña, M., Shephard, M., Velázquez-

- Blazquez, A., Villefranque, N., Wandinger, U., Wang, P., and Wehr, T.: EarthCARE level-2 demonstration products from simulated scenes, <https://doi.org/10.5281/zenodo.7311704>, 2022.
- van Zadelhoff, G.-J., Donovan, D. P., and Wang, P.: Detection of aerosol and cloud features for the EarthCARE atmospheric lidar (ATLID): the ATLID FeatureMask (A-FM) product, *Atmospheric Measurement Techniques*, 16, 3631–3651, <https://doi.org/10.5194/amt-16-3631-2023>, 2023.
- Wandinger, U., Floutsi, A. A., Baars, H., Haarig, M., Ansmann, A., Hünerbein, A., Docter, N., Donovan, D., van Zadelhoff, G.-J., Mason, S., and Cole, J.: HETEAC – the Hybrid End-To-End Aerosol Classification model for EarthCARE, *Atmospheric Measurement Techniques*, 16, 2485–2510, <https://doi.org/10.5194/amt-16-2485-2023>, 2023a.
- Wandinger, U., Haarig, M., Baars, H., Donovan, D., and van Zadelhoff, G.-J.: Cloud top heights and aerosol layer properties from EarthCARE lidar observations: the A-CTH and A-ALD products, *EGUsphere*, 2023, 1–32, <https://doi.org/10.5194/egusphere-2023-748>, 2023b.
- Wehr, T., Kubota, T., Tzeremes, G., Wallace, K., Nakatsuka, H., Ohno, Y., Koopman, R., Rusli, S., Kikuchi, M., Eisinger, M., Tanaka, T., Taga, M., Deghaye, P., Tomita, E., and Bernaerts, D.: The EarthCARE mission – science and system overview, *Atmospheric Measurement Techniques*, 16, 3581–3608, <https://doi.org/10.5194/amt-16-3581-2023>, 2023.
- Weisz, E., Li, J., Menzel, W. P., Heidinger, A. K., Kahn, B. H., and Liu, C.-Y.: Comparison of AIRS, MODIS, CloudSat and CALIPSO cloud top height retrievals, *Geophysical Research Letters*, 34, <https://doi.org/https://doi.org/10.1029/2007GL030676>, 2007.
- Wielicki, B. A. and Coakley, J. A.: Cloud Retrieval Using Infrared Sounder Data: Error Analysis, *Journal of Applied Meteorology and Climatology*, 20, 157 – 169, [https://doi.org/10.1175/1520-0450\(1981\)020<0157:CRUISD>2.0.CO;2](https://doi.org/10.1175/1520-0450(1981)020<0157:CRUISD>2.0.CO;2), 1981.
- Wu, Y., de Graaf, M., and Menenti, M.: The impact of aerosol vertical distribution on aerosol optical depth retrieval using CALIPSO and MODIS data: Case study over dust and smoke regions, *Journal of Geophysical Research: Atmospheres*, 122, 8801–8815, <https://doi.org/https://doi.org/10.1002/2016JD026355>, 2017.
- Yao, Z., Li, J., Weisz, E., Heidinger, A., and Liu, C.-Y.: Evaluation of single field-of-view cloud top height retrievals from hyperspectral infrared sounder radiances with CloudSat and CALIPSO measurements, *Journal of Geophysical Research: Atmospheres*, 118, 9182–9190, <https://doi.org/https://doi.org/10.1002/jgrd.50681>, 2013.
- Yorks, J. E., McGill, M. J., Palm, S. P., Hlavka, D. L., Selmer, P. A., Nowottnick, E. P., Vaughan, M. A., Rodier, S. D., and Hart, W. D.: An overview of the CATS level 1 processing algorithms and data products, *Geophysical Research Letters*, 43, 4632–4639, <https://doi.org/10.1002/2016GL068006>, 2016.